

# Magnetogenesis from Cosmic String Loops

---

Diana Battefeld<sup>1\*</sup>, Thorsten Battefeld<sup>1†</sup>, Daniel H. Wesley<sup>1‡</sup>, Mark Wyman<sup>2§</sup>

<sup>1</sup>*DAMTP, Center for Mathematical Sciences, University of Cambridge, Wilberforce Road, Cambridge, CB3 0WA, UK*

<sup>2</sup>*Perimeter Institute for Theoretical Physics, 31 Caroline St. N, Waterloo, ON, N2L 2Y5, Canada*

PACS 98.80.Cq, 98.54.Kt

ABSTRACT: Large-scale coherent magnetic fields are observed in galaxies and clusters, but their ultimate origin remains a mystery. We reconsider the prospects for primordial magnetogenesis by a cosmic string network. We show that the magnetic flux produced by long strings has been overestimated in the past, and give improved estimates. We also compute the fields created by the loop population, and find that it gives the dominant contribution to the total magnetic field strength on present-day galactic scales. We present numerical results obtained by evolving semi-analytic models of string networks (including both one-scale and velocity-dependent one-scale models) in a  $\Lambda$ CDM cosmology, including the forces and torques on loops from Hubble redshifting, dynamical friction, and gravitational wave emission. Our predictions include the magnetic field strength as a function of correlation length, as well as the volume covered by magnetic fields. We conclude that string networks could account for magnetic fields on galactic scales, but only if coupled with an efficient dynamo amplification mechanism.

---

\*diana.battefeld@helsinki.fi

†tbattefe@princeton.edu

‡D.H.Wesley@damtp.cam.ac.uk

§mwyman@perimeterinstitute.ca

---

## Contents

<b>1. Introduction</b>	<b>2</b>
<b>2. Generating Vortices</b>	<b>4</b>
2.1 Straight Strings	5
2.2 A Rotating Loop	8
<b>3. String Network Models</b>	<b>11</b>
3.1 The one-scale model (OSM)	12
3.2 The velocity-dependent one-scale model (VOS)	13
<b>4. Magnetogenesis and Observational Bounds</b>	<b>14</b>
4.1 Evolution since matter-radiation equality	14
4.2 Analytic Estimates	17
4.2.1 Near decoupling	17
4.2.2 Fields from before Matter domination	18
4.3 Numerical Results	18
4.4 Discussion	19
<b>5. Conclusions</b>	<b>25</b>
<b>A. Dynamics of rotating loops</b>	<b>26</b>
A.1 Changes in size and shape	27
A.2 Translational Movement	27
A.3 Rotational Movement	29
<b>B. Code Implementation</b>	<b>31</b>

---

## 1. Introduction

Large-scale, coherent magnetic fields with strengths in the  $\mu\text{G}$  range are observed in galaxies and clusters [1, 2, 3, 4]. Models that explain the presence of these fields fall into two rough categories: “primordial” mechanisms or “dynamo” mechanisms. The primordial option holds that presently observed fields arose from large-scale, homogeneous fields present soon after the Big Bang. These primordial fields were diluted by cosmic expansion, then slightly amplified by protogalactic collapse to the field strengths presently observed. The dynamo option assumes that very weak “seed” magnetic fields were created by an as-yet-unknown magnetogenesis mechanism in the early universe, which were later greatly amplified by magnetohydrodynamic (MHD) dynamos operating in spiral galaxies.

There are many proposals but few truly compelling mechanisms for primordial magnetogenesis. On the one hand, the primordial option provides an explanation of presently observed magnetic fields, and the required primordial field strength just evades structure formation and cosmic microwave background (CMB) constraints [5, 6, 7, 8, 9, 10, 11]. On the other hand, it is not clear why homogeneous coherent magnetic fields of the correct strength should be present on super-horizon scales. Inflation is one possible cause, but to first order in perturbation theory, the vector perturbations required to create magnetic fields decay with cosmic expansion. Thus any field generation caused by inflationary perturbations must be a second order effect [16]. This initial conditions issue can be circumvented if fields formed on sub-horizon scales after the Big Bang, with field strength transferred to the larger scales needed to account for galactic magnetic fields [1, 3, 13, 14, 15, 12]. Generally the fields produced in this way are very weak, and must be amplified through the action of a galactic dynamo or “inverse cascade” arising from turbulent MHD processes [1, 14, 17]. Ultimately all of these mechanisms come up against the correlation length problem, which itself arises since causal mechanisms can only operate on sub-horizon scales: except for redshifts close to decoupling, such mechanisms produce fields on comoving lengths that are too small to explain the correlation length of fields observed in galaxies and clusters. For most mechanisms, this problem can only be solved by invoking large scale field averaging, inverse cascades, or the super-horizon correlations produced by cosmic inflation. The speculative nature of these proposals is an indication of how challenging it is to generate fields with the proper length scales. In addition, causal mechanisms tend to create fields with a blue power spectrum. If the magnetic fields were created before big bang nucleosynthesis (BBN), then conversion of stochastic magnetic fields into gravitational waves could lead to violations of BBN bounds [18, 19, 20].

In this paper we consider primordial magnetogenesis by a cosmic string network. Such networks are attractive candidates for magnetogenesis, since long strings typically stretch across the cosmological horizon, and so can naturally create coherent effects over large length scales. The motion of strings and loops through the primordial plasma also produces the vector-type perturbations required for generating magnetic fields. Since the magnetic fields are created after BBN, the BBN constraints on stochastic magnetic fields would not apply.

For these reasons and others, cosmic string magnetogenesis has been investigated in the past by a number of others [21, 22, 23]. These works share a common approach, whereby the string network generates vorticity in the primordial plasma, which is subsequently converted to a magnetic field through the Harrison-Rees mechanism [24, 25]. The conversion occurs because electrons and protons experience differing accelerations due to their Compton scattering against CMB photons [25]. This differential vorticity in the plasma creates a current, which then generates magnetic fields. This process operates so long as the Compton scattering of CMB photons from free charged particles is efficient, and so can create magnetic fields until decoupling. Conveniently, in this epoch the cosmological horizon is sufficiently large to produce magnetic fields on comoving scales which are relevant for the generation of today’s galactic and cluster magnetic fields.

We employ a combination of analytic and numerical techniques to estimate the magnetic fields produced by the string network. The central challenge is to obtain an accurate estimate of the vorticity produced by the network. We argue that the vorticity produced by long, horizon-sized strings has been overestimated in the past, and here give improved estimates. We also extend our analysis to include the fields generated by the cosmic string loops produced in string networks. We find that the loops turn out to give the dominant contribution to the total magnetic field produced by the network. In addition to predicting the overall magnetic field strength, we use properties of the string and loop networks to compute the spectrum of field strength as a function of correlation length, as well as the fractional horizon volume coverage of regions in which fields are generated. We obtain these predictions from a computer code which implements two semi-analytic string network models, the one-scale model (OSM) [26] and the velocity-dependent one-scale model (VOS) [27, 28]. The code also incorporates the dynamics of individual loops, including the forces and torques on the loops from Hubble expansion, dynamical friction, and the emission of gravitational waves. We make minimal assumptions about MHD processes, and do not invoke any large scale averaging, inverse cascades, or turbulence.

We find that for reasonable choices of string network parameters, the network can create sufficiently strong seed fields on galactic scales, provided the subsequent dynamo amplification is very efficient. Cosmic string magnetogenesis has the satisfying property that it makes a number of other predictions. We find that adequate magnetic fields can be generated by cosmic strings with tension  $G\mu/c^2 \gtrsim 10^{-8}$ , a value which is still allowed by cosmological observations [29, 30, 31, 32, 33], but may be constrained further by an array of other cosmological observations set to be made within the next few years [34, 35, 36, 37, 38, 39, 40]. Various loop network models give similar predictions for the magnetic field strength as a function of correlation length, and this scale-dependence might be observationally testable. Optimistically, the discovery of cosmic strings with relevant tensions would greatly bolster the viability of this mechanism. On the other hand, if galactic dynamos turn out to be less efficient than we assume, or if no strings with a high enough tension are found, then our mechanism is ruled out.

We organise this paper as follows: in Section 2 we describe our estimates of the vorticity

generated by long string encounters, and discuss the differences between our long string estimates and those in the literature. We also give estimates for the vorticity generated by loops, leaving a detailed discussion of the loop dynamics for Appendix A. Armed with expressions for the vorticity generated by individual strings and loops, we give a brief description of the network models that describe the long string and loop populations in Section 3. We then use this information to present analytic and numerical estimates of the magnetic fields generated by the string network in Section 4. We give the magnetic field strength as a function of correlation length, describe the volume fraction covered by the loops, and discuss how our results depend on the various string and loop network parameters. Some details of the code we developed to obtain these results is given in Appendix B, and we tabulate our parameter choices in Table 2. Our summary and conclusion appear in Section 5. Throughout this work, we set  $c = 1$  but keep other natural constants (such as  $G$ ) explicit.

## 2. Generating Vortices

Long strings generate vorticity by dragging the plasma as they pass through it, and one computes the drag force by calculating the impulse given to test particles by the passing string. This problem is considered in detail in refs. [41, 42, 43, 22, 23], from which we draw some essential facts, summarised below. The simplest situation to study is that of an infinitely long, straight cosmic string with tension  $T$ , fundamental mass per unit length  $\mu_0$ , and effective mass per unit length  $\mu$ . If extended along the  $z$ -axis and moving in the  $x$ -direction with velocity  $v_s$ , it imparts a velocity  $v_y$  to a test particle located far from the  $xz$ -plane, directed toward the  $xz$ -plane and given by

$$v_y = \frac{2\pi G\lambda}{v_s\gamma_s} + 4\pi G\mu_0 v_s \gamma_s. \quad (2.1)$$

where  $\gamma_s = (1 - v_s^2)^{-1/2}$ , and  $\lambda$  is defined as

$$\lambda = \mu - T. \quad (2.2)$$

The effective mass per unit length,  $\mu$ , and tension,  $T$ , are obtained by averaging over the small scale fluctuations, or wiggles, on the string. They are related to the fundamental “bare” tension  $\mu_0$  by [41, 44]

$$\mu T = \mu_0^2. \quad (2.3)$$

Typically  $\mu \approx 1.9\mu_0$  in the radiation era and  $\mu \approx 1.5\mu_0$  in the matter era [45]. Equation (2.1) is valid when we can work in the weak-field limit of GR, when the test particle is far enough from the string that the wiggles can be effectively averaged out, and when the string is moving sufficiently rapidly that the test particle does not move substantially closer to the string during the encounter.

Only the first term in (2.1), which dominates for small string drift velocities  $v_s$ , is important for this work. This term is due to the Newtonian gravitational force of the string: in

linearised GR the Newtonian potential is sourced by both energy density and pressure, so the string creates the same acceleration field as would an infinite rod with linear mass density  $\lambda$  in purely Newtonian gravity. The second term in (2.1) arises from the conical deficit angle  $8\pi G\mu_0$  which the string introduces in the surrounding spacetime. Simulations indicate that wiggles move very quickly, with an RMS velocity of  $v_{RMS} > 0.6$ , and that the velocity of strings averaged over a correlation length is quite small,  $v_s \equiv \bar{v}_{RMS} \approx 0.15$  [41, 46]. So typically the first term dominates, and since  $\gamma_s \approx 1$ , we are safe in using the non-relativistic limit. Therefore we are justified in treating the physics of string encounters with Newtonian gravity. Unlike the conical-deficit approach to long strings, this generalises to loops in a simple and convenient way. It is also a conservative approach, for including the deficit angle contribution leads to stronger plasma flows in the string wake, enhancing the vorticity so produced.

Using the deflection formula (2.1) we re-examine the calculation of vorticity created by long strings in Section 2.1. We then apply the same method to estimate the vorticity generated by string loops in section Section 2.2. We show that producing vorticity by long strings is less attractive than previously thought, but that string loops provide a well-motivated alternative mechanism.

## 2.1 Straight Strings

Long strings generate vorticity by dragging the plasma behind them as they pass through it, or equivalently by producing a velocity component  $v_x$  on test particles. Treated as a first-order perturbation, the  $x$ -component of the force on a test particle vanishes when averaged over the encounter with a string. At second order one includes the motion of the test particle in the  $y$ -direction during the encounter, which brings the particle slightly closer to the  $xz$ -plane during the departure of the string than it was during the approach, resulting in a net force in the  $x$ -direction. The final velocity can be computed [21] by going to the string rest frame, where the test particle moves with velocity  $v_s$ . Since the Newtonian force is conservative, the magnitude of the test particle's velocity is unchanged by the encounter, so

$$v_s^2 = v_y^2 + (v_s - v_x)^2, \quad (2.4)$$

and therefore

$$v_x = \frac{v_y^2}{2v_s} + O(v_y^3). \quad (2.5)$$

To generate magnetic fields, the passing string must generate vorticity in the plasma. After the encounter, matter moves toward the string's trajectory with velocity  $v_y$ , but this flow is not rotational. The plasma's total momentum vanishes after the encounter, due to the symmetry of the flow with respect to the  $xz$ -plane. At second order, the flow created by the drag velocity  $v_x$  has net momentum in the direction of the string movement, but is not rotational either.

A rotational flow can be created by vortices that build up due to turbulence in the string wake, as first proposed by Vachaspati and Vilenkin [41, 42] (see also [47, 21]). The

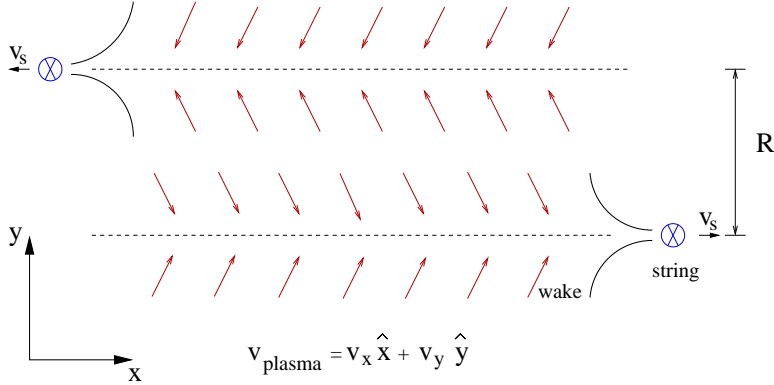


**Figure 1:** Two straight strings with effective Newtonian mass density  $\lambda = \mu - T$  cause wakes in the surrounding plasma via gravitational interaction. After the encounter, the magnitude of the dragging component of the plasma flow velocity is approximately  $v_y \sim G\lambda/v_s$  and  $v_x \sim v_y^2/(v_s)$ . The resulting plasma flow carries a rotational component of velocities up to  $v_{rot} \sim v_x$  over interstring distances, so that an angular frequency of order  $\tilde{\omega}_{pl} \sim \lambda^2 G^2/(R_s v_s^3)$  results, see (2.9).

authors of [21] argue that a two-string encounter creates a vortex whose size is comparable to the interstring distance, with rotational velocities comparable to the infall velocity of the plasma  $v_{rot} \sim v_y$ . Dimopoulos and Davis [22, 23] later investigated the two-string encounter assuming the same plasma flow. The argument they employ runs essentially as follows: plasma of density  $\rho$  in a region of volume  $V \sim R_s^2 v_s T$ , with post-encounter net momentum  $\Delta p \sim R_s^3 \rho v_x$ , leads to a force on the string of  $F \sim \Delta p/T \sim R_s^2 \rho v_y^2$ . Applied over a distance  $R_s$ , the string does work  $W_s \sim \rho R_s^3 v_y^2$ . If we were to assume that the overall flow in the region  $V$  is rotational and were to set  $E_{rot} \sim \rho R_s^3 v_{rot}^2$  equal to  $W_s$ , this would imply  $v_{rot} \sim v_y$ <sup>1</sup>. The keystone of these proposals is the assumption that the vortex size is comparable to the interstring distance, and that it carries the majority of the total kinetic energy imparted to the plasma. As we have shown, such a vortex is not present immediately after the encounter. Indeed, the change in angular momentum of the strings due to the dragging of the plasma is roughly  $\Delta J_s \sim R_s \Delta p \sim R_s^4 \rho v_x$ . Conservation of angular momentum implies that the plasma may have, at most, a rotational component in the volume  $\sim R_s^3$  with angular momentum  $J_{plasma} \sim R_s^4 \rho v_{rot} \sim \Delta J_s$ . Therefore the net rotational velocity is closer to  $v_{rot} \sim v_x$ , which is much smaller than  $v_y$ . This is illustrated schematically in Figure 1.

These estimates can be improved as follows. The wake behind a single string, created at  $t_F \lesssim t_{eq}$ , has a length  $l_w$ , width  $w_w$  and thickness  $d_w$ , given by the scaling relations [48, 49, 45, 50]

$$l_w \sim t_F \frac{z_F}{z}, \quad w_w \sim v_s t_F \frac{z_F}{z}, \quad d_w \sim v_y t_F \left( \frac{z_F}{z} \right)^2, \quad (2.6)$$

<sup>1</sup>An additional factor of 2 in [23] stems from taking  $v_{rot} \sim u \equiv 2v_y$ , where  $u$  is the relative velocity of particles on opposite sides of the string.

which are valid for  $z > z_F v_y / v_s$ . Turbulent eddies arise within the wake shock [47], and could potentially lead to large rotational velocities of order  $v_y$ . However, the characteristic size associated with matter chunks due to fragmentation of the wake is comparable with the thickness of the wake  $d_w$  behind an individual string [52, 51, 45]. We expect turbulent, gravitationally supported vortices at this length scale. Comparing this thickness to the interstring distance  $R_s(t) \sim P^\beta v_s t$  yields

$$\frac{d_w}{R_s} \sim \frac{v_y t_F (z_F/z)^2}{v_s P^\beta t} \sim 2\pi \sqrt{\frac{z_F}{z}} \frac{G\lambda}{v_s^2 P^\beta}, \quad (2.7)$$

where we use  $v_y$  from (2.1),  $P$  is the intercommutation probability <sup>2</sup>,  $1/2 \leq \beta \leq 1$  [46], and  $t_F/t = (a_F/a)^{3/2} \sim (z/z_F)^{3/2}$ . Considering mildly relativistic strings ( $v_s \sim 0.1$  as an order of magnitude) and the largest possible  $G\lambda \sim 10^{-7}$ , we are left with

$$\frac{d_w}{R_s} \sim 2\pi \sqrt{\frac{z_F}{z}} \frac{10^{-5}}{P^\beta}. \quad (2.8)$$

Below we show that the vortices relevant for magnetogenesis are created toward the end of the radiation era, so the redshifting factor is of order unity and vortices due to turbulence in the string wake are much smaller than the interstring distance. The seed fields necessary to initiate plausible galactic dynamos should be coherent over distances of at least  $\xi_{seed} \sim 5 - 50$  pc at decoupling, but  $d_w \sim 1$  pc for turbulent eddies created around  $t_{dec}$ . We discuss the relevant length scales in more detail in Section 4.

Since the magnetic field is directly proportional to the angular velocity of the plasma, our new estimate greatly reduces the expected strength of magnetic fields produced by the long strings. Our arguments indicate that the drag velocity  $v_x$  is the relevant velocity for magnetic fields that are coherent over interstring distances, not the infall velocity  $v_y$ . This gives a plasma vorticity

$$\omega_{pl} \sim \frac{v_x}{R_s} \sim \frac{v_y^2}{2R_s v_s} \sim \frac{(2\pi)^2 \lambda^2 G^2}{2R_s v_s^3}. \quad (\text{long strings, this paper}) \quad (2.9)$$

This is in contrast with [22, 23] which obtains the estimate

$$\omega_{pl}^{[23]} \sim \frac{v_y}{R_s} \sim \frac{2\pi \lambda G}{v_s R_s}. \quad (\text{long strings, previous}) \quad (2.10)$$

We find that while rotational velocities  $\sim v_y$  are possible within the string wake, by (2.8) their correlation length is much smaller than the interstring distance  $R_s$ .

To summarize: vortices due to turbulence in the string wake are confined to small scales, much smaller than the interstring distance  $R_s$ . Even though these vortices may have large rotational velocities, their small size makes them far less appealing for magnetogenesis.



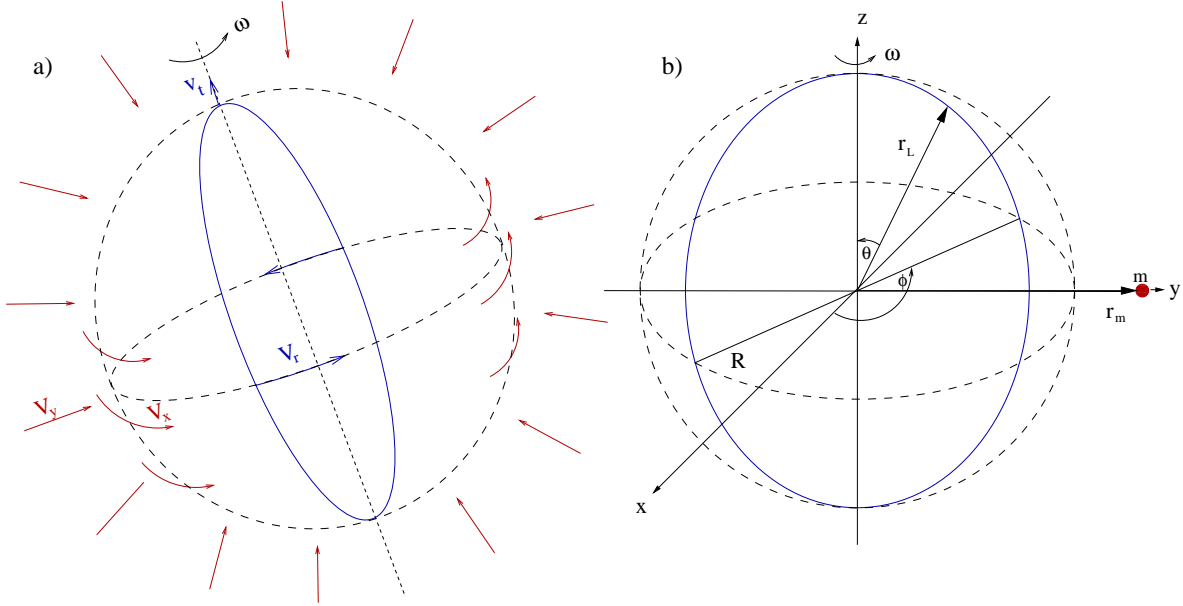


**Figure 2:** a) A rotating loop with angular velocity  $\omega$  and drift velocity  $v_t$  attracts the surrounding plasma with a net velocity of order  $v_y \sim G\lambda/v_t$ , which in turn causes a vortex with rotational velocity of order  $v_x \sim v_y^2/v_r$  over the size of the loop. The resulting angular velocity of the plasma is of order  $\omega_{pl} \sim \lambda^2 G^2 / (\ell v_t^2 v_r)$ , see eqn. (2.25). b) Schematic of a rotating loop at  $\mathbf{r}_L(\sigma, t)$  and a test mass at  $\mathbf{r}_m$ . Here  $\phi = \omega t$ ,  $\theta = \pi\sigma$ .

## 2.2 A Rotating Loop

We now consider the generation of rotational velocity flows in the plasma by a loop instead of a long string. We make the assumption that a loop in a typical state of motion has a nonzero angular velocity  $\omega$ . The drag force from the loop then transfers angular momentum to the plasma in a straightforward fashion. The correlation length of the rotational flow, and thus of the magnetic field, is set by the size of the loop. In this section we estimate the resulting vorticity.

As in the long string case, our first task is to compute the gravitational impulse exerted on a test particle by a passing rotating loop. We consider a rigid, circular loop of radius  $R$ , length  $\ell = 2\pi R$ , and linear mass density  $\lambda$ , with its angular velocity  $\omega$  and translational velocity  $v_t$  oriented along the  $z$ -axis. This situation is illustrated in Figure 2. Analytic solutions to the loop equations of motion are known [54], but in general the loop dynamics are quite complex, and certainly we do not expect cosmic string loops to act precisely as the rigid loops we study here. Nonetheless, we assume that the relevant physics operating on the largest loop length scales is effectively captured by the idealization of a rigid loop, and its “coarse-grained” properties such as velocity, angular momentum, mass and size. The parameters  $\ell$ ,  $v_r$  and  $v_t$  are all functions of time, thanks to the dynamical forces acting on the loop and its emission of gravitational radiation. We describe the equations that govern these

---

<sup>2</sup> $P \approx 1$  for cosmic strings,  $10^{-1} \leq P \leq 1$  for D-strings and  $10^{-3} \leq P \leq 1$  for F-strings [53].

quantities in Appendix A, and find that  $\ell$ ,  $v_r$  and  $v_t$  change very little over the timescales associated with test particle encounters. While we take all of these dynamical forces into account when studying the long-term evolution of the loop population, for the purpose of estimating the drag on the plasma, we treat  $\ell$ ,  $v_r$  and  $v_t$  as constants.

Switching to the loop's rest frame, we consider a particle at  $\mathbf{r}_m = \tilde{R}\hat{\mathbf{y}}$ . At time  $t$ , we parameterise points  $\mathbf{r}_L$  on the loop by

$$\mathbf{r}_L = R \begin{pmatrix} \sin \pi \sigma \cos \omega t \\ \sin \pi \sigma \sin \omega t \\ \cos \pi \sigma \end{pmatrix} \quad (2.11)$$

where  $\sigma$  ranges over  $-1 \dots 1$ . We take the ratio

$$\mathcal{R} = \frac{\tilde{R}}{R} \quad (2.12)$$

to be larger than, but close to, unity. We further define the displacement  $\mathbf{d} = \mathbf{r}_L - \mathbf{r}_m$  with magnitude

$$d = R \left( 1 - \frac{2y_m}{R} \sin \pi \sigma \sin \omega t + \frac{y_m^2}{R^2} \right)^{1/2}. \quad (2.13)$$

Recalling that we have defined  $x$  as the direction parallel to the string's motion, we know that the acceleration component  $a_x$  vanishes to first order if we average over a full rotation. The net acceleration is in the  $y$ -direction, toward the loop, and given by

$$a_y = \pi G \lambda R \int_0^1 d\tau \int_{-1}^1 d\sigma \frac{d_y}{d^3} = \mathcal{C}_1 \pi \frac{G \lambda}{R}, \quad (2.14)$$

where  $\tau = t/T$ , with  $T$  the loop rotation period  $T = 2\pi/\omega$  and

$$\mathcal{C}_1 \equiv R^2 \int_0^1 d\tau \int_{-1}^1 d\sigma \frac{d_y}{d^3}, \quad (2.15)$$

which is of order one. (For example, one finds  $\mathcal{C}_1 \approx -1/2$  for  $\tilde{R} = 2R$ ). The net velocity toward the loop after one rotation is then

$$v_y \approx \frac{2\pi}{\omega} |a_y| = |\mathcal{C}_1| 2\pi^2 \frac{G \lambda}{v_r} \sim \pi^2 \frac{G \lambda}{v_r}. \quad (2.16)$$

Thanks to its drift velocity  $v_t$ , the loop undergoes roughly  $4R\omega/(2\pi v_t) = 2v_r/(\pi v_t)$  rotations before it moves away from the test particle, so the total velocity acquired by the test particle during the encounter is

$$v_y \sim \frac{2\pi G \lambda}{v_t}, \quad (2.17)$$

which is similar to the straight string case in (2.1). Only the translational velocity  $v_t$  enters this expression, since the longer a particle experiences the gravitational attraction toward the loop, the faster they approach each other in the end.

The drifting loop drags the plasma behind it – just as a straight string does – but unlike the string encounter, the flow has a rotational component. The drag velocity in the  $x$ -direction is again of order  $v_x \sim v_y^2/v_t$  (see below), resulting in a dynamical friction force on the loop of  $F \sim R^2 \rho v_y^2 \sim R^2 \rho G^2 \lambda^2 / v_t^2$ . This has two effects on the loop. First, it feels a net force due to dynamical friction of [55, 56]

$$\dot{v}_t = -\frac{v_t}{t_*} \ln \theta_{min}^{-1} \quad (2.18)$$

where

$$\theta_{min} = \frac{2G\lambda\ell}{v_t^2 r_{max}} \quad (2.19)$$

is the minimum scattering angle,  $r_{max} = \int v_t dt \simeq 3vt$ , and

$$t_* = \frac{v_t^3}{8\pi^2 G^2 R \lambda \rho}. \quad (2.20)$$

Second, because the loop rotates, the drag force generates a vortical flow. As in the long string case, this is a second-order effect. The acceleration in the  $x$ -direction due to an infinitesimal element of the loop  $d\sigma$  is

$$da_x = \frac{\pi G \lambda R^2}{d^3} \sin \pi \sigma \cos \omega t d\sigma \quad (2.21)$$

Substituting the first-order trajectory of the test particle, given by

$$y_m(t) = \tilde{R} + v_y \left( t - \frac{\pi}{\omega} \right) \quad (2.22)$$

with  $y_m(\pi/\omega) = \tilde{R}$ , into (2.21), expanding in terms of  $\varepsilon \equiv v_y(t - T/2)/R \ll 1$ , computing the drag velocity by integrating the first order term over a single period (the zeroth order contribution vanishes due to symmetry), and replacing  $G\lambda$  in terms of  $v_y$  results in

$$v_x \approx \frac{v_y^2}{v_r} |\mathcal{C}_2| \sim \frac{v_y^2}{7 v_r}, \quad (2.23)$$

where

$$\begin{aligned} \mathcal{C}_2 \equiv & 12\pi \int_{-1}^1 d\sigma \int_0^1 d\tau \sin \pi \sigma \cos 2\pi \tau \left( \tau - \frac{1}{2} \right) \\ & \times \frac{\mathcal{R} - \sin \pi \sigma \sin 2\pi \tau}{(1 + \mathcal{R}^2 - 2\mathcal{R} \sin \pi \sigma \sin 2\pi \tau)^{5/2}}. \end{aligned} \quad (2.24)$$

Numerical integration gives  $\mathcal{C}_2 \approx -0.14$  for  $\mathcal{R} = \tilde{R}/R = 2$ , so we take  $\mathcal{C}_2 = -1/7$ . The drift velocity  $v_t$  enters (2.23) via  $v_y \sim 2\pi G\lambda/v_t$ , so as a result of the drag force, the plasma is stirred up with angular velocity

$$\omega_{pl} \sim \frac{v_x}{\ell} \sim \frac{v_y^2}{7\ell v_r} \sim \frac{(2\pi)^2 \lambda^2 G^2}{7\ell v_t^2 v_r}, \quad (\text{loops}) \quad (2.25)$$

where we take the vortex size to be given by the loop length  $\ell = 2\pi R$ . For comparison, the vorticity due to straight string encounter, derived in Section 2.1, is

$$\omega_{pl} \sim \frac{v_x}{R_s} \sim \frac{v_y^2}{2R_s v_s} \sim \frac{(2\pi)^2 \lambda^2 G^2}{2R_s v_s^3}, \quad (\text{long strings}) \quad (2.26)$$

where  $R_s$  denotes the interstring distance  $R_s \approx P^\beta v_s t$ .

We show in Appendix A that  $v_r(t)$  and  $v_t(t)$  are comparable to the average velocity of straight strings,  $v_s$ . Therefore the ratio of vorticities is essentially controlled by the ratio  $\ell/R_s$  of loop length to long string separation. Since the loop must linger in each region of space long enough to establish a vortex, vortices are only created when  $v_r > v_t$ .

In this section we focus entirely on the generation of vorticity, since it is a precondition for the Harrison-Rees mechanism to create magnetic flux. Since these vortices are real astrophysical objects, they are subject to many physical processes which we have not considered here, and our comparisons of the length scales and vortex velocities should be viewed in this light. For instance, though there is a small vortical component to the plasma flow in the region between two widely separated cosmic string wakes, this vast distance will encompass many local over- and under-dense regions, complicating the physics. On the other hand, the length scales perturbed by string loops and single string vortices are somewhat smaller, and should thus be less subject to the vagaries of small plasma variations. Furthermore, in each case the strings are doing more than generating vortical motions and magnetic fields: they are accreting matter themselves. This adds to local overdensities, and makes the regions overswept by strings somewhat more likely later to collapse and develop structure. We should also have string loops attracted to relatively overdense areas. We may thus expect regions that have been affected by string magnetogenesis to be, preferentially, those regions which later form structure. Though small, we believe this phenomenon will help to increase the effective coverage of string-sourced magnetic fields, since even if they fail to cover the whole universe, the parts that they do cover will likely be the parts that will eventually host galaxies.

### 3. String Network Models

To obtain a prediction for magnetogenesis, we must combine our results for the magnetic fields from a single loop or string, obtained in Section 2, with a model of the network population. We use the model to provide the loop length spectrum, defined by

$$N(\ell, t) = \frac{dN_{loops}}{d \ln \ell} \quad (3.1)$$

where  $\ell$  is the loop length and  $N_{loops}$  the number of loops per comoving Hubble volume. To explore the dependence of our results on network model assumptions, we use two popular semi-analytic loop network models: the one-scale model (OSM) and the velocity-dependent one-scale model (VOS). Both models obtain equations for the evolution of the long string energy density, and then apply energy conservation to determine the energy fed into the loop population in the form of newly formed loops.

### 3.1 The one-scale model (OSM)

According to the OSM [26, 43, 45] the absolute number of loops  $N_{loops}$  in a physical volume  $V(t)$  obeys the equation

$$\frac{dN_{loops}}{dL_H(t)} = \frac{V(t)}{L_H(t)^4} \frac{C}{\alpha} \quad (3.2)$$

where  $C$  is constant during matter- or radiation-dominated epochs,  $\alpha$  is the size of newly created loops as a fraction of  $L_H(t)$ , and

$$L_H(t) = a(t) \int_0^t \frac{dt'}{a(t')} \quad (3.3)$$

is the particle horizon measured in physical units. A loop formed at time  $t_F$  is taken to have initial length  $\ell(t_F) = \alpha L_H(t_F)$ , and then subsequently loses energy through the emission of gravitational radiation. The length at time  $t$  of a loop formed at  $t_F > t$  is given by

$$\ell(t, t_F) = f_r \alpha L_H(t_F) - \Gamma_\ell G\mu(t - t_F) \quad (3.4)$$

where  $f_r$  represents the energy loss from the redshifting of the loop peculiar velocity immediately after formation, and  $\Gamma_\ell$  is a dimensionless parameter controlling the efficiency with which the loop emits gravitational radiation.

Using the fundamental OSM equations (3.2,3.4) we now compute  $N(\ell, t)$ . To integrate (3.2) we take  $V(t) = (a(t)R)^3$ , so (3.1) measures the absolute number of loops per (cubical) comoving volume  $R^3$ . As we are primarily concerned with the radiation dominated epoch, we take  $L_H(t) = 2t = 1/H(t)$ . To calculate  $N(\ell, t)$  we first rewrite (3.1) as

$$N(\ell, t) = \frac{dN_{loops}}{dL_H(t_F)} \frac{dL_H(t_F)}{d \ln \ell}. \quad (3.5)$$

By (3.4), a loop currently of length  $\ell$  at time  $t$  must have formed at a time  $t_F$  when the particle horizon  $L_H(t_F)$  was

$$L_H(t_F) = 2 \left( \frac{\ell + \Gamma_\ell G\mu ct}{2\alpha f_r + \Gamma_\ell G\mu} \right), \quad (3.6)$$

which yields the second factor in (3.5) by differentiation. To obtain the first factor, we pick a fiducial time  $t_0$  during radiation domination, set  $a(t_0) = 1$ , and fix  $R = L_H(t_0)$ . This yields

the number of loops per logarithmic interval in  $\ell$ , at time  $t$ , in a comoving volume equal to one Hubble volume at a time  $t_0$ , as

$$N(\ell, t) = \frac{30}{\alpha} \left( \alpha f_r + \frac{\Gamma_\ell G\mu}{2} \right)^{3/2} \frac{L_H(t_0)^{3/2} \ell}{\left( \ell + \frac{\Gamma_\ell G\mu}{2} L_H(t) \right)^{5/2}} \quad (3.7)$$

where we have taken the value  $C \sim 30$  during radiation domination, as in [26]. Despite the fact that new loops are being created at  $\ell = \alpha L_H$ , the spectrum possesses a peak at the characteristic length

$$\ell_{peak}(t) = \frac{\Gamma_\ell G\mu}{2} L_H(t) \sim 50 \cdot G\mu \cdot ct \quad (3.8)$$

taking  $\Gamma_\ell \sim 50$  [26, 79, 80]. The spectrum falls off for  $\ell > \ell_{peak}$  since the large loops are created during times of slower loop production, and falls off for  $\ell < \ell_{peak}$  since the small loops are near the end of their lives and are evaporating rapidly. Similar expressions can be derived in the matter era.

### 3.2 The velocity-dependent one-scale model (VOS)

The VOS model of refs. [27, 28] characterises the string population by a length scale  $L$ , a velocity  $v$ , and a string number density  $n$ . Commonly, one makes the approximation  $n \equiv L^{-2}$ , but for our code we maintain these as distinct parameters for flexibility. Like the OSM model, the VOS model has several dimensionless parameters, which we call  $c_1, c_2$ , and  $c_3$ . These are fixed by matching to numerical simulations. Taking from [27] the scaling values of  $HL$  and  $v$ , we find  $c_1 = 0.21$  (0.2475),  $c_2 = 0.18$  (0.3675) in the radiation (matter) eras. We allow free evolution of the network in the dark energy era using matter era parameters, as this epoch does not effect magnetogenesis. The third parameter,  $c_3 = 0.28$ , fixes the scaling string number density. The physical origin of these equations and their parameter inputs is discussed extensively in ref. [27]; matching between the equations presented here and those of ref. [27] is explained in ref. [28]. The VOS model assumes that the length scale evolves according to

$$\frac{dL}{dt} = HL + c_1 v \quad (3.9)$$

where the loop parameter  $c_1 \leq 1$  is dimensionless. The velocity  $v$  obeys

$$\frac{dv}{dt} = \frac{-2Hv + c_2/L}{1 - v^2}, \quad (3.10)$$

and the comoving number density of long strings  $N = a^2 n$  is governed by

$$\frac{dN}{dt} = -\frac{c_2 N v}{L} - \frac{c_3 N^2 L v}{a^2}. \quad (3.11)$$

To translate the output of these equations into what we want – namely, loop creation rates – requires a further step. Taking  $\rho_\infty = n\mu$ , we can just plug the rate of change of cosmic string

energy density into the loop creation rate formula from ref. [26],

$$\frac{dN_{loops}}{dt} = -\frac{V(t)}{\mu\alpha L_H(t)} \left[ \dot{\rho}_\infty + 2\frac{\dot{a}}{a}\rho_\infty (1 + \langle v^2 \rangle) \right], \quad (3.12)$$

where in this formula  $L_H$  is again the horizon size,  $V$  is the horizon volume, and  $\alpha$  is, again, the size of the loops after creation as a fraction of  $L_H$ .

## 4. Magnetogenesis and Observational Bounds

We now gather our preliminary results to determine whether the string network can account for the magnetic fields observed today. In Section 4.1 we follow the evolution of the fields from decoupling, through galaxy formation, to the operation of a dynamo mechanism. In Section 4.2 we give analytic estimates for the resulting galactic fields, followed by our numerical results in Section 4.3. There are great uncertainties affecting almost every stage of the evolution of magnetic fields – especially the dynamo amplification efficiency – but we show that with an efficient dynamo it is possible to account for presently observed galactic magnetic fields. We summarise our parameter choices in Table 2, found on page 37.

### 4.1 Evolution since matter-radiation equality

The vorticity created by the cosmic string network sources magnetic fields through the Harrison-Rees mechanism [24, 25]. Harrison [24] was the first to consider a model whereby a seed field is generated by a vortex in the ionized plasma. In Harrison’s model, a circular current develops when there is a differential rotational flow between ions and the electron-photon gas. Due to Thompson scattering, non-relativistic electrons are tightly coupled to the radiation bath before  $t_{dec}$ . Ions are not tightly coupled, so expansion damps their angular momentum more efficiently. Because the electrons outpace the ions, a net current is set up which generates a magnetic field. Rees [25] pointed out that Harrison’s mechanism creates vortices that decay too quickly in the radiation era to produce useful fields, and suggested a modification. Rees’ mechanism relies on vortical flows in the early matter era, when vortical motion is less destabilized by expansion. Since the plasma is still optically thick before recombination, the angular velocity of the electron fluid is damped through Compton drag caused by the microwave background; meanwhile the relatively heavy ions are less affected. Again, a current is established, though in a direction opposite that of Harrison’s original proposal. The strength of a magnetic field produced in this way is [21]

$$B = \frac{2m}{e}\omega_{pl} \approx 10^{-4}\omega_{pl}, \quad (4.1)$$

where  $B$  is in Gauss and  $\omega_{pl}$  in  $s^{-1}$ . This mechanism can only produce magnetic fields when the universe is ionised and Compton scattering is efficient, which ceases to be true after decoupling. Though it is also true that the universe reionised at low redshift, the Harrison-Rees mechanism no longer works in the late universe since the radiation density is low, rendering Compton scattering ineffective.

Once magnetic fields are produced at a redshift  $z_F$ , their (proper) correlation length  $\xi$  grows with the expansion of the universe as

$$\xi(z) = \frac{1+z_F}{1+z} \xi(z_F), \quad (4.2)$$

and their field strength evolves according to

$$B(z) = \left( \frac{1+z}{1+z_F} \right)^2 B(z_F), \quad (4.3)$$

as a consequence of flux conservation. Once galaxy formation begins, the evolution of magnetic fields becomes far more complicated. As a protogalactic cloud becomes non-linear and begins to collapse, the correlation length decreases but the field strength is amplified. While there may be some amplification of the field during collapse [57, 58], we assume that no dynamo is active at this stage and the field strength is primarily governed by flux conservation [59, 60]. The net predynamo amplification factor in a spiral galaxy is approximately [15]<sup>3</sup>.

$$\frac{B_i}{B_{gf}} \approx 8 \times 10^3, \quad (4.4)$$

where  $B_{gf} = B(z_{gf})$ . Once the protogalactic cloud collapses, we assume that the field is amplified exponentially by a dynamo mechanism [15], such as the  $\alpha\omega$ -dynamo<sup>4</sup>. This dynamo begins operation when stellar winds and explosions generate interstellar turbulence, which transforms into cyclonic motions through the Coriolis forces associated with galactic rotation [61, 62]. The magnetic field surrounding the galaxy has two modes, a toroidal and a poloidal component. The dynamo converts the poloidal to toroidal flux by differential rotations of the galactic disk (the  $\omega$ -effect) and the toroidal to poloidal through the cyclonic motions (the  $\alpha$ -effect) [63]. The combined effects can amplify the magnetic field strength by many orders of magnitude [64, 65, 66, 15].

We parameterise the dynamo by an efficiency factor  $\Gamma_{dy}$ , such that  $\Gamma_{dy}^{-1}$  is the field strength  $e$ -folding time, and the field  $B_0$  measured today is related to the initial field  $B_i$  by

$$\ln \frac{B_0}{B_i} = \Gamma_{dy} (t_f - t_i) \quad (4.5)$$

where  $t_i \gtrsim t_{gf}$  indicates the onset of dynamo amplification,  $t_f \lesssim t_0$  is the time at which the fields reach the observed value, and  $t_{gf}$  is the time at which the protogalactic cloud collapses. We take  $t_i = t_{gf}$  and  $t_f = t_0$  to arrive at the most optimistic lower bound of the seed field. The resulting amplification is weakly sensitive to the choice of  $t_{gf}$ , and here we take  $t_{gf} = 475$  Myr, which corresponds to  $z_{gf} = 10$ .

Although the value of  $\Gamma_{dy}$  is crucial to estimate the necessary seed field, its value is a matter of considerable debate. In the literature, one finds many values for  $\Gamma_{dy}$  scattered in

---

<sup>3</sup>This expression includes: formation of a halo, gain of angular momentum through tidal interactions with neighbouring galaxies, and disc formation, see [15] for a review.

<sup>4</sup>The  $\alpha\omega$ -dynamo assumed here applies to galactic magnetic fields growing in discs only.



galaxy formation		$\Gamma_{dy}^{-1}$			
$z_{gf}$	$t_{gf}$	0.2 Gyr	0.3 Gyr	0.5 Gyr	1.0 Gyr
6	1 Gyr	$3.8 \times 10^{27}$	$2.4 \times 10^{18}$	$1.1 \times 10^{11}$	$3.3 \times 10^5$
10	475 Myr	( $\star$ ) $5.2 \times 10^{28}$	$1.4 \times 10^{19}$	$3.1 \times 10^{11}$	$5.5 \times 10^5$

**Table 1:** The amplification factor  $B_0/B_i$ , tabulated with a variety of assumptions regarding the time  $t_{gf}$  and redshift  $z_{gf}$  of galaxy formation and the efficiency  $\Gamma_{dy}$  of the galactic dynamo. The value we take to get the most optimistic lower bound on  $B_{seed}$  in (4.6) is marked with a “ $\star$ .”

the range  $0.2 \text{ Gyr} < \Gamma_{dy}^{-1} < 0.8 \text{ Gyr}$  [68, 64, 67]. Recently, some have contended that even larger values,  $\Gamma_{dy}^{-1} \gtrsim 1.1 - 1.4 \text{ Gyr}$ , are more likely [15]. Still, taking this uncertainty as an opportunity for optimism, we consider very efficient dynamos with  $\Gamma_{dy}^{-1} = 0.2 \text{ Gyr}$ , which amplify by a factor  $5.2 \times 10^{28}$  (the amplification factors for various choices of  $\Gamma_{dy}$  and  $t_{gf}$  are given in Table 1; note that in the numerical results that follow, §4.3,  $\Gamma_{dy}^{-1} = 0.3 \text{ Gyr}$  will be adequate). To obtain the present field of  $B_0 = 10^{-6} \text{ Gauss}$  under these assumptions, the field  $B_{seed}$  that must be present at decoupling with  $z_{dec} = 1089$  is

$$B_{seed} \approx 2 \times 10^{-35} \text{ G}. \quad (4.6)$$

This is a very optimistic lower bound for the seed field at  $t_{dec}$ . For seed fields between this limit and  $10^{-20} \text{ G}$ , only the most efficient dynamos might work, though the existence of such dynamos in nature is controversial [15].

In addition to constraints on its strength, the seed field must possess a sufficiently large correlation length. The correlation length after protogalactic collapse  $\xi_{gf}$  must satisfy  $\xi_{gf} \geq 100 \text{ pc}$  for the dynamo to commence [60]. Using a simple spherical collapse model for galaxy formation to estimate the comoving correlation length  $x_{corr}$  before galaxy collapse leads to [60]

$$x_{corr} > \eta x_{gal} = 0.95 \eta (\Omega_m h^2)^{-1/3} M_{12}^{1/3} [\text{Mpc}] \quad (4.7)$$

where  $M_{12} = M/10^{12} M_\odot$ ,  $M$  is the mass of the galaxy,  $x_{gal}$  is the comoving length of the galaxy at formation, and  $\eta$  is the fraction of a galaxy over which the magnetic field has to be correlated. Taking  $M_{12} \approx 0.1$  and  $\eta \approx 1/150$  (corresponding to  $\xi_{gf} \approx 100 \text{ pc}$ ) yields

$$x_{corr} \approx 5.8 \text{ kpc}. \quad (4.8)$$

Consequently, the seed fields must have a physical correlation length  $\xi_{seed}$  at decoupling of

$$\xi_{seed} = \frac{x_{corr}}{1 + z_{dec}} > 5.4 \text{ pc}. \quad (4.9)$$

which compares favorably with the particle horizon of  $\approx 200 \text{ kpc}$  at  $z \approx 1000$ . Larger seed field correlation lengths are even better: the 5.4 pc minimum quoted here should cover only about 10% of the protogalactic cloud, which is only marginally adequate. A seed field with a longer length scale – say 50 pc – would comfortably suffuse the whole protogalactic cloud with a single coherent field.

## 4.2 Analytic Estimates

### 4.2.1 Near decoupling

Straight string encounters near decoupling produce vorticity given by  $\omega_{pl}$  from (2.26), which by the Harrison-Rees mechanism creates a seed field of

$$B_s \sim 10^{-4} (2\pi)^2 \frac{(\mu - T)^2 G^2}{2v_s^3 R_s} \lesssim 1.6 P^{-\beta} \times 10^{-26} \text{ G}, \quad (4.10)$$

where we use  $G(\mu - T) \leq 10^{-7}$ ,  $v_s \geq 0.1$  and an interstring distance of  $R_s = P^\beta v_s t_{dec}$ . These fields have a correlation length at decoupling of

$$\xi_s \sim 12 P^\beta \text{ kpc}. \quad (4.11)$$

The field strength in (4.10) is several orders of magnitude smaller than the corresponding one in [23], since our estimates of the vorticity on large scales generated by a two-string encounter is much lower than that in [23]. Cosmic strings with  $P^\beta \sim 1$  and the largest possible string tension produce fields that are just strong enough to seed the most efficient dynamos. This improves somewhat for F and D-strings, which can have a lower  $P^\beta$ . In either case the coherence length is larger than the minimal one in (4.9).

The vorticity from rotating loops with  $\omega_{pl}$  from (2.25) results in seed fields of

$$B_\ell \sim 10^{-4} \frac{(2\pi)^2 (\mu - T)^2 G^2}{7 \ell v_t^2 v_r}. \quad (4.12)$$

Taking  $G(\mu - T) \leq 10^{-7}$ ,  $v_t \geq 0.1$ ,  $v_r \approx 0.4$  and defining a new parameter  $\tilde{\alpha}$  such that the loop length  $\ell$  at formation is

$$\ell = \tilde{\alpha} t_F = \frac{f_r \alpha}{H(t_F)}, \quad (4.13)$$

at  $t_F = t_{dec}$  we obtain

$$B_\ell \lesssim \frac{2.9 \times 10^{-29}}{\tilde{\alpha}} \text{ G}. \quad (4.14)$$

We use  $v_t \geq 0.1$  since even a large initial velocity of  $v_t \sim v_{RMS}$  decreases due to redshifting in the matter era, before it speeds up again due to the rocket effect (see Appendix A.2). Because redshifting is absent for the rotational movement, the rotational velocity decreases only very slowly due to the emission of gravitational waves, which is also counterbalanced by loop shrinking to some extent (see Appendix A.1); hence we use  $v_r \approx 0.4$  (Appendix A.3). Since  $\tilde{\alpha} < P^\beta v_s$ , we can achieve a larger field strength than for a straight string encounter. Consequently, less efficient dynamos work, but not all galaxies are so lucky as to have had a loop sweeping over them in the past. The coherence length

$$\xi_l \sim 117 \tilde{\alpha} \text{ kpc}. \quad (4.15)$$

is large enough to seed the dynamo for  $\tilde{\alpha} \geq 10^{-5}$ , so that both the largest loops and many of the smaller ones contribute to magnetogenesis. The smaller the loops, the stronger the resulting seed field.

The analytic estimates suggest similar contributions in magnetic field flux from long strings and loops. In fact, the numerical estimates presented in Section 4.3, which include more details of the loop dynamics and population characteristics, show that loops produce much stronger magnetic field fluxes than long strings. Partly this is because the loop length spectrum peaks at lengths much smaller than  $\alpha L_H$ , which effectively lowers the value of  $\tilde{\alpha}$  and greatly increases the fields they create. In addition, redshifting slows the loops, which then create stronger magnetic fields.

#### 4.2.2 Fields from before Matter domination

Extending magnetogenesis into the era before matter domination is a tricky business. As one pushes to higher redshift, the horizon becomes ever smaller, and sufficient correlation lengths even harder to achieve. Also, having more expansion time for vortices and magnetic fields to dilute pushes the predicted field strengths from these earlier times to even lower and less plausible values. In addition, many dissipative processes are present in this era, causing both  $B$  and  $\xi$  to decrease further; as a consequence, it is unlikely that any primordial magnetic fields within the horizon survive with reasonable strength and coherence length [70]. To complicate matters even more, the full set of MHD equations should be used deep in the radiation era [69], instead of the simple scaling laws. We conclude that magnetic fields with the largest fluxes and correlation lengths are the ones created around decoupling.

### 4.3 Numerical Results

The mechanism for magnetogenesis presented here involves too much physics to be treated efficiently using only analytic methods. But each of the relevant physical effects is reasonably well studied, so we include them using a computer code. The code is discussed in more detail in Appendix B. Briefly, the advantages of using the code include:

- Loops are dynamical objects, and a code can track their evolution over time.
- The fraction of the universe’s volume that is given a seed field is very important to know, yet very difficult to estimate analytically. In a code, this can easily be computed.
- String parameters – like the bare tension  $G\mu_0$ , and  $\alpha$ , the loop size – enter the equations in a variety of places, making it hard to guess how magnetogenesis strength, length scales, and volume coverage will be affected by each. Our code allows us simply to try a variety of values and compare the outcomes to develop some intuition about their effects.
- The relative sizes of loop and straight string contributions to magnetogenesis are easy to calculate and compare on equal footing, without making the possibly prejudicial approximations necessary for analytical estimation.

The model parameters we wish to vary are:

1.  $G\mu_0$ , the string’s bare tension;
2. our model for string network evolution;
3. whether or not string loops are allowed to undergo dynamics;
4. the initial velocity at which a loop moves after formation;
5.  $\alpha$ , the average length of a new loop after it has formed.

This last parameter is under very active study at present from both analytical [71, 72, 73] and numerical [74, 75, 76, 77] perspectives. It is an important thing to understand because large loops live much longer than small loops. Loops lose their length by generating gravitational radiation, which is now beginning to be brought under observational limits; since longer loops emit gravity waves later, they are more tightly constrained (see ref. [78] for much more detail). For the discussion of our numerical results, we first treat them as free and independent parameters so as to study how each affects magnetogenesis. On the other hand, we take our test values for  $G\mu_0$  from observational constraints: a fiducial value of  $2 \times 10^{-7}$  [29, 30], an optimistic value of  $7 \times 10^{-7}$  [31], and the most constrained value of  $2 \times 10^{-8}$  [32]; the former two come from combining CMB data with other cosmological observations, while the last is the “worst case scenario” limit from pulsar timing. At the end of this section, we present constraints on what we consider to be the best motivated combination of parameters, which differs slightly from our fiducial model. Our fiducial model, used wherever nothing else is specified, includes: the VOS model for long strings; loop dynamics turned on;  $G\mu_0 = 2 \times 10^{-7}$ ;  $\alpha = 0.01$ ; and  $v_t(t = t_F) = 0.1$ . Where relevant, we have drawn a line demarcating the minimum correlation length necessary to seed galactic dynamos and a line indicating the minimum magnetic field strength necessary, given a particular dynamic amplification time,  $\Gamma_{dy}^{-1}$ .

#### 4.4 Discussion

We now discuss the results of the numerical simulations. Unless stated otherwise, all of the plots assume the VOS model with loop dynamics,  $G\mu_0 = 2 \times 10^{-7}$ ,  $\alpha = 0.01$ , and  $v_t(t = t_F) = 0.1$ . We have systematically explored the variation of our predictions with the parameters listed above.

The scaling of the magnetic field spectrum with  $G\mu_0$ , illustrated in Figures 3, can be understood within the context of the calculations in Sections 2 and 3. As  $G\mu_0$  is reduced, each loop becomes less effective at generating magnetic fields, and so the magnetic flux is reduced. Furthermore, the loop length spectrum peaks at a characteristic length determined by  $G\mu_0$ , as given in (3.8) for the OSM model. Since we use only a single scale for loop formation here, we find the same result in the VOS model. As  $G\mu_0$  is reduced, this characteristic loop size falls as well, shifting the magnetic field spectrum to smaller correlation lengths.

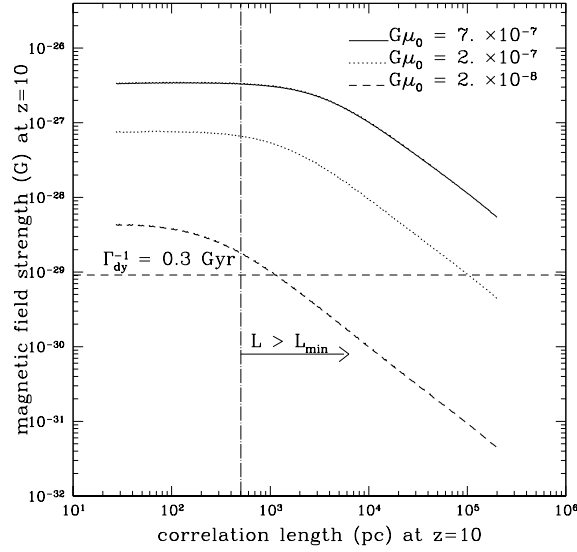


**Figure 3:** Magnetic field strength as a function of the magnetic field’s correlation length, for our three test values of bare string tension  $G\mu_0$ . The plot shows the magnetic field strength at  $z = 10$  as a function of the proper correlation length at the same redshift.

The magnetic field strength as a function of correlation length for several values of  $\alpha$

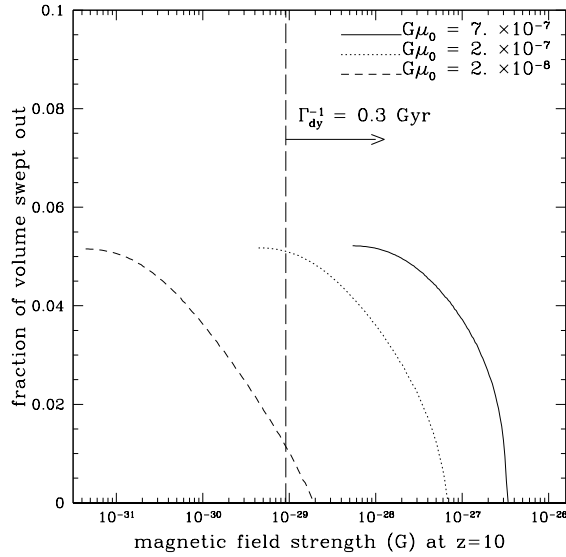


**Figure 4:** Volume of universe suffused with a seed field as a function of seed field flux magnitude. The horizontal axis gives the magnetic field strength at  $z = 10$ , and the vertical axis shows the fraction of the volume of the universe which is suffused with a magnetic field of that flux or greater.

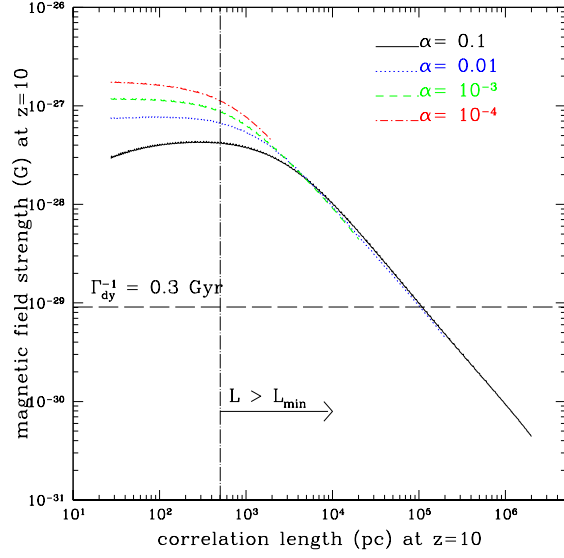


**Figure 5:** Magnetic field strength as a function of the string formation length fraction  $\alpha$ .

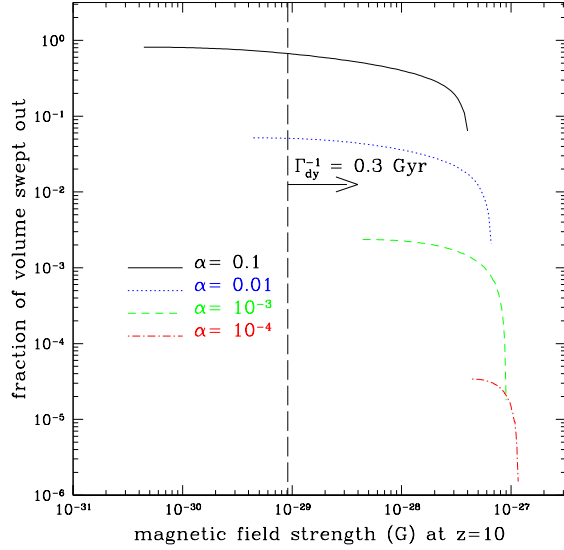


**Figure 6:** Volume of universe suffused with a seed field as a function of seed field flux magnitude, for various values of  $\alpha$ .

is given in Figure 5. The magnetic field spectrum is only weakly dependent on  $\alpha$ , thanks primarily to two effects. First, while  $\alpha$  sets the size of the largest loops, at any fixed time the greatest number of loops have characteristic length that is set by  $G\mu_0$ , as described for the OSM model in (3.8). Therefore the peak correlation length and magnetic field flux only weakly depend on  $\alpha$ . Secondly, loops created in models with larger  $\alpha$  will always shrink to

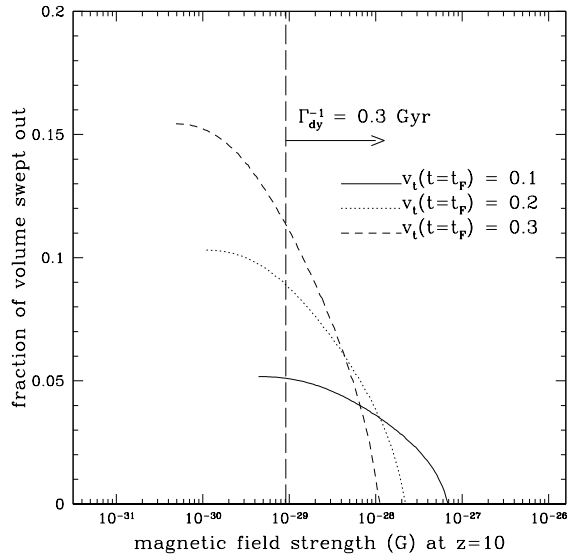


**Figure 7:** Volume of universe suffused with a seed field as a function of seed field flux magnitude, for various values of the loop’s initial translational velocity,  $v_t(t = t_F)$ .

smaller lengths, and thus mimic models in which  $\alpha$  is smaller. The peak magnetic flux grows slightly with  $\alpha$ , since at progressively smaller values of  $\alpha$ , the string network must shed energy into an ever greater number of ever smaller loops. Thus, the fraction of loops creating fields at the peak correlation length grows slowly as  $\alpha$  decreases.

To provide a viable magnetogenesis mechanism, cosmic string loops must not only produce sufficiently strong magnetic fields, but must produce them over nearly the entire volume of the universe. Figures 4, 6, and 7 explore this issue for different values of  $G\mu_0$ ,  $\alpha$ , and loop  $v_t$  at formation. In these figures, we have plotted the fraction of a universe suffused with a given magnetic field strength or greater. If one chooses a value of magnetic flux required to seed a galactic dynamo, the curves give the fraction of the universe in which the string network produces the required seed fields. Figure 4 shows the same fall in peak magnetic field strength with falling  $G\mu_0$  as does Figure 3. Beyond shifting to smaller values of magnetic field strength, the curves look roughly similar: as  $G\mu_0$  is decreased, the loop network contains roughly the same number and sizes of loops, which produce the same volume coverage but lower magnetic field strengths. Figure 6 shows the same weak dependence of the peak magnetic field strength on  $\alpha$  as does Figure 5. The volume coverage falls nearly linearly with  $\alpha$ , as is to be expected since at smaller values of  $\alpha$  the loop network contains fewer large loops. The scaling, very roughly speaking, is that the volume swept out by a single loop is proportional to  $\alpha^2$ , while the number of loops produced is proportional to  $\alpha^{-1}$ , the combination of which gives an approximately linear scaling of volume with  $\alpha$ . Finally, in 7, we see an approximately linear scaling in volume coverage with loop initial transverse velocity. Faster loops can sweep out more volume, but since they remain in any one area for a shorter period of time, they

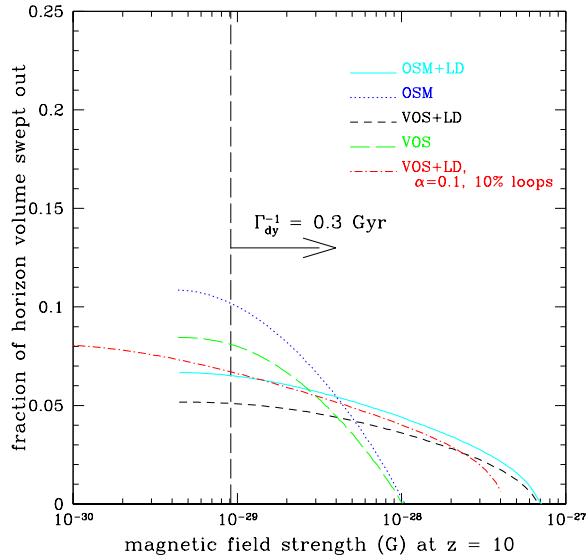


**Figure 8:** Since loops change their size over time, different volumes of space will be endowed with seed fields of differing magnitudes. Here we plot a line indicating the percent of the universe covered by a magnetic field whose size is greater than or equal to some minimum field strength. Results for both network models are shown for comparison, and for each we show results both with (+LD) and without loop dynamics. To explain a bit better, an example: the point where the red line crosses 8% is at a magnetic field strength of approximately  $10^{-30}$  G. What this means is that 8% of the volume of the universe at the time of galaxy formation was suffused with a seed field whose magnitude was equal to, or larger than,  $10^{-30}$  G. Here we have adopted  $G\mu_0 = 2 \times 10^{-7}$  and  $\alpha = 10^{-2}$ . Only fields whose correlation lengths are sufficiently large ( $L_{corr} > 500\text{pc}$  at  $z = 10$ ) are included. We have also included what we believe to be the best motivated model: the VOS model for the long strings, loop dynamics, and  $\alpha = 0.1$ , but with only 10% of the string network’s energy loss going into loops that large, with the rest lost to very small loops.

produce weaker magnetic fields. This is also evident in the plot.

Figures 8, 9, and 10 explore the effect of loop dynamics and the network model on our conclusions. In Figure 8, we plot the horizon volume overswept versus the magnetic field strength, as in Figures 4, 6, 7 above. Two effects are evident in these results. The One Scale Model covers a slightly large volume of the universe with fields than the Velocity-dependent One Scale model, as the OSM tends to overestimate the number of long strings present during the matter-radiation transition era, leading to a greater number of loops present during magnetogenesis. The inclusion of loop dynamics increases magnetic field strength but decreases volume coverage, since loop dynamics decrease loop translational velocity over time. In addition to these model comparisons, we also plot the model we believe to have the best physical motivation: the VOS model, with loop dynamics included, where string loops are formed at 10% of the horizon size, but with only 10% of the loop energy going into loops this large. We assume that the remaining 90% of loops are formed near the gravitational radiation



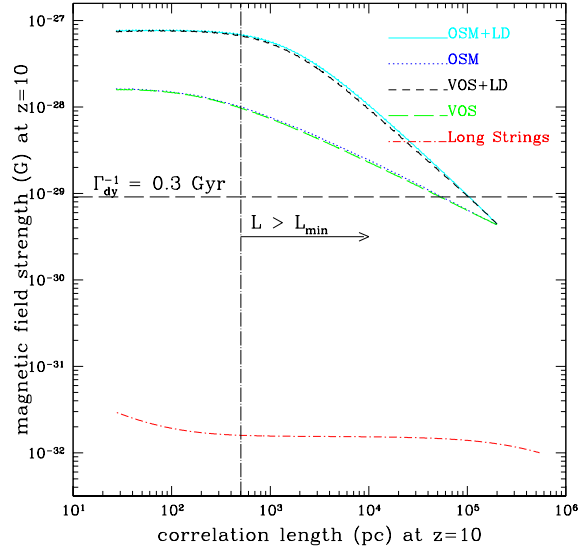


**Figure 9:** Magnetic field strength for the different string models we consider, excluding our best motivated physical model (which on this plot is nearly identical with VOS+LD), compared with the prediction from long string encounters, where the vortex is created in the region between two oppositely moving long strings.

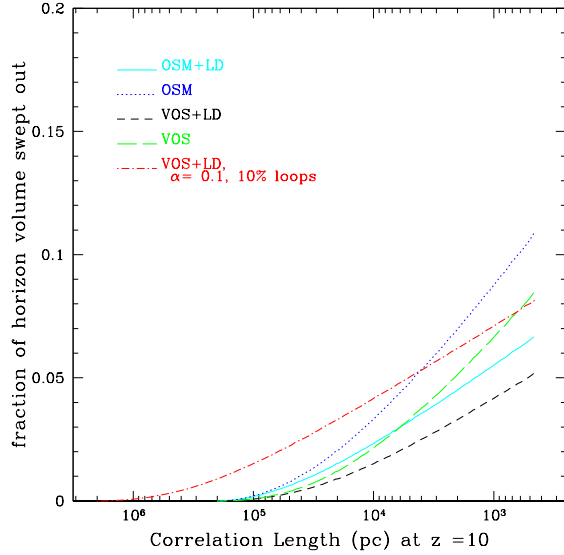


**Figure 10:** For the five model combinations we consider, we plot the fraction of the volume covered versus the correlation length. Only fields whose correlation lengths are sufficiently large ( $L_{corr} > 500\text{pc}$  at  $z = 10$ ) are included.

back-reaction scale, through loop fragmentation or other effects [78]. In Figure 9, we compare the magnetic field strengths in our models with the magnetic fields expected from long string encounters. Since the vortices formed by long string encounters are spread over such large length scales, the fields generated by those encounters are concomitantly much weaker than those generated by loops. Finally, in Figure 10, we plot volume overswept versus correlation length for these same five models, beginning with the largest correlation lengths. This plot includes only field correlations lengths that are sufficiently large ( $L_{corr} > 500\text{pc}$  at  $z = 10$ ).

## 5. Conclusions

In this paper, we have studied the viability of a cosmic string network for generating the seed fields necessary for explaining, after dynamic amplification, the  $\mu G$  magnetic fields observed in spiral galaxies. We have analyzed the behavior of wiggly cosmic strings in the era between matter-radiation equality and decoupling. In this era, we find that strings can create vorticity in the primordial plasma, allowing the Harrison-Rees mechanism for magnetogenesis to operate. This effect is, however, at second order in the string’s effective Newtonian mass density, contrary to earlier estimates in the literature. Though the turbulent eddies in wakes behind long strings can form stronger magnetic fields, by our calculations these fields are on length scales too small to explain galactic magnetic fields. On the other hand, we find only weak support in our calculations for vortices forming in the space between distantly separated straight strings, which would have adequate correlation lengths.

However, by interpolating between these extremes, we have discovered that cosmic string loops provide an excellent mechanism for magnetogenesis, with correlation length scales that are large enough as well as field strengths much greater than those predicted for the speculative inter-string vortices. If we take present work on loop production seriously, then approximately 10% of the energy a string network loses goes into strings whose length is approximately  $0.1L_H$ . These loops can oversweep approximately 10% of the universe during the relevant epoch between matter-radiation equality and decoupling. With loops preferentially oversweeping areas with overdensities, this may be just enough coverage. Also, if cosmic strings are  $(p, q)$  strings from string theory, we can expect a further enhancement of this volume coverage by a factor of approximately  $3P^\beta$  [28]. In those regions that are overswept, strings with tensions allowed by present-day cosmological constraints can generate seed magnetic fields large enough to account for today’s magnetic fields under the assumption of an efficient galactic dynamo for amplification. Although we are making optimistic assumptions about these dynamos, we have consistently made conservative estimates for the string-driven magnetogenesis. For instance, we are not forced to rely on turbulence or inverse cascades to achieve these results; if such mechanisms exist, then the seed fields we predict would only be strengthened.

We achieved these predictions first through careful analytical estimation, then through the construction of a thorough computer code. This latter has allowed us to simultaneously solve for the evolution of the string network, loop production, loop dynamics, and cosmology,

giving us predictions for magnetic fields that take into account a multitude of effects. Beyond a bare estimate of the magnetic field amplitude, we correlate the volume of the universe overswept by loops with such parameters as  $G\mu_0$ , the string tension, and  $\alpha L_H$ , the typical size of loops. In addition, we compare the results of two popular semi-analytic string network models, the original one scale model as well as the more sophisticated velocity-dependent one scale model. Because of the versatility supplied by the code, we predict, inter alia, the spectrum of magnetic field strength versus correlation length. Though it may be far fetched, if future astronomical observations were capable of detecting and characterizing the primordial seed field, our predictions are sufficiently concrete that such observations could either confirm or refute our model.

In addition to futuristic observations, our model could also be refuted through the definitive disproof of efficient galactic dynamos (our model requires  $\Gamma_{dy}^{-1} \lesssim 0.3$ ), or the constraint of cosmic string tensions to much less than  $G\mu \simeq 10^{-8}$ . On the other hand, if cosmic strings are observed and possess a tension of around our fiducial value, the case for this magnetogenesis mechanism would be greatly strengthened.

Thus, the presence of a string network might help explaining some large scale magnetic fields if efficient galactic dynamos are present. Put in other words, with efficient galactic dynamos, we can explain a  $\mu\text{G}$  with a  $G\mu$ .

## Acknowledgments

We thank S. Alexander for early discussions motivating this project as well as A. C. Davis and K. Dimopoulos for feedback, especially regarding the role of turbulence in string wakes. D.W. and M.W. thank the University of Sussex for their wine and hospitality during the completion of this work. T. B. is supported by PPARC grant PP/D507366/1 and thanks the Perimeter Institute for their hospitality. The work of M. W. at the Perimeter Institute is supported in part by the Government of Canada through NSERC and by the Province of Ontario through MEDT. D. B. would like to thank A. C. Davis and DAMTP for support.

## A. Dynamics of rotating loops

Loops are acted upon by dynamical friction forces as well as the recoil and shrinking from the emission of gravitational waves. We must estimate these effects to ensure that the approximations we make in Section 2.2 are valid, as well as to properly incorporate them in the numerical estimates presented in Section 4.3 and described in detail in Appendix B. In this Appendix we derive the differential equations that govern the evolution of the translational velocity  $v_t(t)$ , rotational velocity  $v_r(t)$  and length  $\ell(t)$  of a loop, and provide approximate analytic solutions.

## A.1 Changes in size and shape

The length of the loop decreases due to gravitational radiation, so that

$$\ell(t) = f_r \alpha L_H(t_F) - \Gamma_l G \mu_0 (t - t_F) \quad (\text{A.1})$$

$$\equiv \ell_0 - G \Gamma_l \mu_0 (t - t_F), \quad (\text{A.2})$$

where  $f_r \leq 1$  describes energy loss directly after formation,  $\Gamma_l \approx 50$  controls the efficiency with which the loop emits gravitational radiation [26, 79, 80],  $\ell_0 \equiv \tilde{\alpha} t_F = f_r \alpha L_H(t_F)$ , and the time scale for loop shrinkage is

$$t_{shrink} \equiv \frac{\tilde{\alpha}}{G \Gamma_l \mu_0} t_F = 2000 t_F, \quad (\text{A.3})$$

for  $\tilde{\alpha} = 0.01$  and  $G \mu_0 = 10^{-7}$ ; so a loop with  $\tilde{\alpha} > 10^{-5}$  remains large enough for magnetogenesis for many Hubble times.

A further concern is large-scale loop oscillations, which change the shape of the loop significantly. (Small scale oscillations of the string are already averaged over to give the effective tension  $T$  and linear mass density  $\mu$ ). If the oscillation timescale is comparable to the rotation period, the rigid loop approximation does not apply. Since the initial velocity distribution on the loop has to be quite peculiar to yield a fast oscillation affecting the loop as a whole, we expect that these oscillations make only a small fraction of loops unsuitable.

## A.2 Translational Movement

Three effects determine the drift velocity of a loop: redshifting from Hubble expansion, dynamical friction due to dragging of the plasma as computed in (2.18), and recoil from gravitational wave emission [81] (often referred to as the *rocket effect*). The latter causes an acceleration of  $\Gamma_p G \mu_0 \hat{\mathbf{n}}/\ell$ , where  $\hat{\mathbf{n}}$  is a unit vector in the direction of recoil and  $\Gamma_p \approx 10$  [81]. (It is  $\mu_0$  and not  $\lambda = \mu - T = \mu(1 - \mu_0^2/\mu^2) \approx 0.56\mu_0$  which determines the emission of gravitational waves.) Incorporating these forces leads to

$$\dot{\mathbf{v}}_t = -H \mathbf{v}_t - \frac{\mathbf{v}_t \ln \theta_{min}^{-1}}{t_*} + \frac{\Gamma_p G \mu_0}{\ell} \hat{\mathbf{n}}, \quad (\text{A.4})$$

where  $t_*$  is defined in (2.20) and  $\theta_{min}$  in (2.19). In the matter era, using  $H = 2/(3t)$  and  $8\pi G \rho = 3H^2$  gives

$$t_* \equiv \frac{v_t^3 t^2}{C_1}, \quad C_1 = \frac{2}{3} G \ell \lambda. \quad (\text{A.5})$$

Since our arguments in the previous subsection show that the loop length  $\ell$  decreases very little over the timescales we are interested in, we take  $\ell$  to be a constant. Further, we ignore the time dependence in the logarithm and estimate this factor by <sup>5</sup>

$$\ln \theta_{min}^{-1} \approx \ln \left( \frac{3v_t^3(t_F)t_F}{2G\ell\lambda} \right) = \text{const}, \quad (\text{A.6})$$

---

<sup>5</sup>We approximate  $r_{max} = \int v_t dt \approx 3v_t t \approx 3v_t(t_F)t_F$ , anticipating  $v_t \propto 1/a \propto 1/t^{2/3}$  initially, due to redshifting.

where the time of loop creation is

$$t_F = \ell/\tilde{\alpha}. \quad (\text{A.7})$$

Different initial values can lead to great differences in the long-term behavior of  $v_t$ . The loop either slows rapidly, or accelerates quickly to relativistic velocities from the rocket effect. Below we integrate the dynamical equation (A.4) in each regime, and derive the limiting velocity  $v_{lim}$  that separates the two regimes. Without the rocket effect term, equation (A.4) becomes

$$\dot{v}_t = -\frac{2}{3t}v_t - \frac{C_1 \ln(\theta_{min}^{-1})}{t^2 v_t^2}, \quad (\text{A.8})$$

which has the solution

$$\begin{aligned} v_t^f(t) &= t^{-2/3} \left( -3C_1 \ln(\theta_{min}^{-1})t + \frac{\ell}{\tilde{\alpha}^2} (3C_1 \ln(\theta_{min}^{-1})\tilde{\alpha} + v_0^3 \ell) \right)^{1/3} \\ &\approx v_0 \left( \frac{\ell}{\tilde{\alpha}t} \right)^{2/3} \left( 1 - \frac{t}{t_f} \right)^{1/3} \end{aligned} \quad (\text{A.9})$$

where the last step uses  $v(t_F) = v_0$ , neglects  $3C_1 \tilde{\alpha} \ln(\theta_{min}^{-1})$ , and employs the time scale of dynamical friction defined by

$$t_f \equiv \frac{v_0^3 \ell}{2\lambda G \tilde{\alpha}^2 \ln(\theta_{min}^{-1})}. \quad (\text{A.10})$$

When dynamical friction is irrelevant (A.4) becomes

$$\dot{v}_t = -\frac{2}{3t}v_t + C_2, \quad (\text{A.11})$$

where  $C_2 \equiv \Gamma_p G \mu_0 / \ell$  and we assume that the recoil is collinear with the velocity. This has the solution

$$\begin{aligned} v_t^r(t) &= \frac{1}{5t^{2/3}} \left( 3C_2 t^{5/3} - \frac{\ell^{2/3}}{\tilde{\alpha}^{5/3}} (3\ell C_2 - 5v_0 \tilde{\alpha}) \right) \\ &\approx v_0 \left( \frac{\ell}{\tilde{\alpha}t} \right)^{2/3} \left( 1 + \left( \frac{t}{t_r} \right)^{5/3} \right), \end{aligned} \quad (\text{A.12})$$

where we neglect  $3\ell C_2$  in the last step and introduce the relevant time scale  $t_r$  for the rocket effect

$$t_r \equiv \left( \frac{5v_0}{3\Gamma_p G \mu_0} \right)^{3/5} \frac{\ell}{\tilde{\alpha}^{2/5}}. \quad (\text{A.13})$$

Setting  $t_r = t_f$  and solving for the initial velocity yields

$$v_{lim} = G^{1/6} \left( \frac{\lambda^5}{\mu_0^3} \right)^{1/12} \left( \frac{5}{3\Gamma_p} \right)^{1/4} 2^{5/12} \tilde{\alpha}^{2/3} (\ln \theta_{min}^{-1})^{5/12}, \quad (\text{A.14})$$

Hence, for  $v_t \ll v_{lim}$  dynamical friction is more important, whereas for larger velocities, the rocket effect predominates in the long run.

What is a reasonable initial value for  $v_t$ ? If large loops are created in the matter era, we expect their velocities to be comparable to the RMS velocity in the string network  $v_{RMS} \sim 0.6$ <sup>6</sup>. If we average over the small scale wiggles, the RMS velocity drops down to  $\bar{v}_{RMS} \sim 0.15$  [41], so the initial translational velocity of the loops should be smaller too. Rotating loops share kinetic energy between translation and rotation, so an initial value of  $v_t \sim v_r$ , say down to 0.4, may be reasonable. This velocity is still larger than the limit velocity (A.14), even for the largest loops produced in the network: for  $\tilde{\alpha} = 0.01$  and the bound  $G\lambda/0.56 = G\mu_0 \lesssim 10^{-7}$ , the limiting velocity becomes  $v_{lim} \lesssim 0.0072$ , where we approximated  $\ln\theta_{min}^{-1} \approx 19$ , based on (A.6) with  $v_t(t_F) = 0.4$ . Hence, the translational velocity of loops which are created in the matter era is given by

$$v_t(t) \approx v_0 \left( \frac{\ell}{\tilde{\alpha}t} \right)^{2/3} \left( 1 + \left( \frac{t}{t_r} \right)^{5/3} \right), \quad (\text{A.15})$$

for all relevant values of  $\tilde{\alpha}$ . The loop initially slows due to redshifting, even though the rocket effect dominates over dynamical friction. Indeed, for  $\tilde{\alpha} \sim 0.01$ ,  $v_0 = 0.4$  and  $\Gamma\mu_0 = 10^{-7}$  we have  $t_r \approx 197\ell/\tilde{\alpha} = 197t_F$ . In this case,  $v_t$  drops down to the minimal value of  $v_t \approx 0.024$  at  $t \approx t_r 3/4$ , and it increases linearly thereafter up until loop shrinking becomes important. Since it takes more than  $1000t_F$  for a loop to accelerate so that it moves faster than  $v_0$  again, we expect the majority of loops to have a translational velocities of order  $v_t \sim \mathcal{O}(10^{-1})$ , which we use as a rough estimate of  $v_t$  for loops created between  $t_{eq}$  and  $t_{dec}$ . Since  $t_r < t_{shrink}$  from (A.3), our assumption of a fixed loop length  $\ell$  is justified.

### A.3 Rotational Movement

The rotational velocity  $v_r$  of a loop is influenced by three effects: dynamical friction from plasma drag, emission of gravitational radiation<sup>7</sup> which produces a torque [82]

$$\tau_{gr} = -\ell G\mu_0^2 \Gamma_{gr} \quad (\text{A.16})$$

where  $\Gamma_{gr} \approx 5$  [82], and the shrinking of the loop from gravitational wave energy emission. The torque  $\tau_{drag}$  from dynamical friction is computed using the arguments of Section 2.2, applied to a single loop rotation. During one rotation, spanning a time  $\Delta t \sim \ell/v_r$ , the surrounding plasma acquires an angular momentum of roughly

$$\Delta J \sim \ell \Delta p_{plasma} \sim \ell^4 \rho v_x \sim \frac{\ell^4 \rho v_y^2}{7v_r} \quad (\text{A.17})$$

---

<sup>6</sup>Recent simulations and analytic arguments suggest two distinct classes of loops [72, 78]: small, highly relativistic loops, and large ones, which have the velocities we consider.

<sup>7</sup>There is no rocket effect for angular momentum: numerical studies show that the emission of gravitational waves always decreases the angular momentum [82], even though a rigorous mathematical proof is lacking. The fundamental mass density  $\mu_0$  determines this effect and not the effective mass density  $\lambda$ .

which gives the torque

$$\tau_{drag} \approx -\frac{(2\pi)^2}{7} \frac{G^2 \lambda^2}{v_r^2} \ell^3 \rho. \quad (\text{A.18})$$

Loop shrinkage enters via the expression for the total angular momentum  $J$ ,

$$\dot{J} = \frac{\lambda}{4\pi} \left( 2\ell \dot{v}_r + \ell^2 \ddot{v}_r \right), \quad (\text{A.19})$$

with  $\ell(t)$  from (A.2). We neglect redshifting of the rotational velocity for loops well within the horizon.

Unlike the translational velocity, it is possible to obtain analytic solutions for the rotational velocity with dynamical  $\ell(t)$ . Dynamical friction is negligible, since the ratio of torques is

$$\frac{\tau_{drag}}{\tau_{gr}} = \frac{(2\pi)^2}{7} \frac{\lambda^2 \tilde{\alpha}^2}{\mu_0^2 v_r^2 \Gamma_{gr} 6\pi} \frac{t_F^2}{t^2} \approx 1.3 \times 10^{-5} \frac{t_F^2}{t^2} \ll 1 \quad (\text{A.20})$$

where we use  $8\pi G\rho = 4/(3t^2)$  as well as  $\lambda/\mu_0 \sim 0.6$ ,  $\tilde{\alpha} \sim 0.01$ ,  $v_r \sim 0.4$  and  $\Gamma_{gr} \approx 5$ . This leaves  $\dot{J} = \tau_{gr}$ , leading to

$$\dot{v}_r = \frac{2G\Gamma_l \mu_0 v_r(t) - C_{gr}}{\ell_0 - G\Gamma_l \mu_0 (t - t_F)}, \quad (\text{A.21})$$

where

$$C_{gr} = \frac{4\pi G \mu_0^2 \Gamma_{gr}}{\lambda}, \quad (\text{A.22})$$

and  $\ell(t)$  is given by (A.2). Assuming the initial condition  $v_r(t_F) = v_0$ , then  $v_r(t)$  is

$$v_r(t) = \frac{1}{2} \frac{C_{gr} f(t) + 2v_0 \tilde{\alpha}^2}{G\Gamma_l \mu_0 f(t) + \tilde{\alpha}^2} \quad (\text{A.23})$$

with

$$f(t) \equiv 2\tilde{\alpha} \left( 1 - \frac{t}{t_F} \right) + G\Gamma_l \mu_0 \left( 1 - \frac{t}{t_F} \right)^2. \quad (\text{A.24})$$

As with the translational velocity  $v_t$ , there is a critical initial rotational velocity that determines the future evolution of  $v_r$ , given by  $v_{lim}^r \equiv C_{gr}/(2G\Gamma_l \mu_0)$ . For the parameters in table 2 we get  $v_{lim}^r > 1$ , indicating that  $v_r$  decreases for all loops under consideration.

What is the initial velocity of a loop? Loops can be produced by self-intersections of a single string. In this case, we expect the intersecting pieces to move roughly in the same direction. As a consequence, the majority of the energy will go into translational movement and a loop with very little angular momentum but large momentum results, so that  $v_r \ll v_t$ . However, Loops can also be created when two strings, moving in opposite directions, intersect and chop off a loop. Loops formed in this way have very little momentum, but large angular

momentum, so that initial rotational velocities comparable to the RMS velocity of the network result  $v_r \approx v_{RMS}$ , while  $v_t \ll v_r$ .

An ideal loop for magnetogenesis lies somewhere in between. Optimally efficient loop magnetogenesis requires rotation to stir up the plasma, but also rapid translational motion to oversweep a large fraction of the universe. To account for kinetic energy in the form of the small scale wiggles and oscillations of the loop, as well as the angular momentum that is radiated away in gravitational waves immediately after its creation, we take  $v_r \sim 0.4 < v_{RMS}$  to be a conservative initial value.

## B. Code Implementation

To fully account for the background cosmological model, the forces and torques on rotating loops, and the behavior of the string/loop network when the universe is not in a scaling regime, we employ a computer program which implements the full set of differential equations described in this paper. Here we discuss the operation of this code.

The code follows an array of loop cohorts over time, while simultaneously tracking some averaged quantities describing the cosmological model and network of long strings. At each time step, the code updates the background cosmological quantities (Hubble parameter, energy density components, *etc.*) according to the Friedmann and energy conservation equations. It also updates the properties of the long string network by using either the one-scale model (Section 3.1) or the velocity-dependent one-scale model (Section 3.2). Both the OSM and VOS models include a production rate for loops at a size determined by the background cosmological parameters, so in each time step the appropriate number of loops are added to the corresponding cohort in the array.

In each time step we include all of the physics of the loop dynamics and magnetic field generation for each loop cohort. Each individual cohort collects all the loops created during a block of time steps. We typically use  $10^6$  steps equally spaced in  $\log(t)$  from redshifts  $z \approx 10^8$  until the present, with blocks consisting of  $10^3$  steps each. The loops created during each time block have similar properties, but there are slight differences between the loops added at the beginning and end of a single block. The code accounts for these differences by updating some of the cohort parameters through a weighted average of the properties of the newly added loops and the properties of the loops already in the cohort. Each cohort tracks a number of different variables:

1. The comoving number density of loops in the cohort, as computed by the OSM (3.2) or VOS equations (3.12). The comoving number density is not averaged at each time step, but accumulates new loops as they are created.
2. The physical length of the loops in the cohort, which decreases due to the emission of gravitational radiation, with the rate given by (3.4). This is averaged over the cohort.
3. The translational and rotational velocity of the loops, which are computed using (A.4) and (A.19), respectively. This includes Hubble damping, the rocket effect, dynamical



friction, torque from gravitational wave emission, and the shrinking moment of inertia of the loops. These properties are averaged over the cohort.

4. The fractional comoving volume overswept by the loops in the cohort, which depends on the comoving number density and translational velocity of the loops. This is a proxy for the fraction of the universe over which the loops in the cohort may generate magnetic fields, and is accumulated (not averaged) as new loops are added.

At each time step, the program updates each of these quantities, from the time the first loops are added to the cohort until the cohort has completely evaporated into gravitational radiation.

The ultimate objective is to calculate the magnetic field strength as a function of scale created by the loops. This is tabulated in an array which tracks the comoving magnetic fluxes  $a^2(t)B(t)$  on a selection of length scales. Each magnetic field bin also tracks the fractional comoving volume of the universe which contains magnetic fields at that length scale. An individual loop cohort generates magnetic fields on large comoving scales when the loops are newly created, and then on progressively smaller scales as the loops shrink. Furthermore, the magnetic field at each comoving correlation length gets contributions from many different loop cohorts over time. Therefore the array tracking magnetic field strengths is indexed differently from the one tracking the loop cohorts, with each array element corresponding to a fixed range of comoving lengths.

At each time step, the code steps through the loop cohorts, and assigns the magnetic fields generated by each cohort in that time step to a bin in the magnetic field array, determined by the size of the loops in the cohort. The comoving magnetic flux is then updated by averaging the flux already present and the flux created by the loops in the cohort, weighted by the comoving volume traversed by the loops in the cohort and the total comoving volume already present in the bin. The comoving volume represented by the bin is incremented by the volume traversed by the loop cohort over the last time step. At the end of the simulation each bin in the magnetic field array represents the average magnetic field strength in a certain fraction of the universe over which the field is correlated over a given length.

To compare the field created by the loop population to that created by the long strings, a parallel calculation tracks the magnetic field created by the long string population. This is much simpler than the loop calculation, primarily because the correlation length for long-string magnetic fields is given by the interstring separation, which is usually some nearly constant fraction of the horizon length. Thus each comoving correlation length only gets contributions from a fixed moment in cosmic history.

## References

- [1] D. Grasso and H. R. Rubinstein, *Phys. Rept.* **348**, 163 (2001) [arXiv:astro-ph/0009061].
- [2] C. L. Carilli and G. B. Taylor, *Ann. Rev. Astron. Astrophys.* **40**, 319 (2002) [arXiv:astro-ph/0110655].
- [3] M. Giovannini, arXiv:astro-ph/0612378.
- [4] M. Giovannini, *Int. J. Mod. Phys. D* **13**, 391 (2004).
- [5] Ya. Zeldovich, *Sov. Phys. JETP* **21**, 656 (1965)
- [6] L. Grishchuk, A. Doroshkevich and I. Novikov, *Sov. Phys. JETP* **28**, 1210 (1969).
- [7] P. J. Peebles, *Astrophys. J.* **147** (1967) 859.
- [8] M.J. Rees and M. Rheinhardt, *Astr. Ap.* **19**, (1972) 189.
- [9] I. Wasserman, *Astrophys. J.* **224** (337) 1978.
- [10] J. D. Barrow, P. G. Ferreira and J. Silk, *Phys. Rev. Lett.* **78**, 3610 (1997) [arXiv:astro-ph/9701063].
- [11] R. Durrer, T. Kahniashvili and A. Yates, *Phys. Rev. D* **58**, 123004 (1998) [arXiv:astro-ph/9807089].
- [12] L. Malyskin and R. M. Kulsrud, *Astrophys. J.* **571** (2002) 619-637, astro-ph/0202284.
- [13] P. P. Kronberg, *Rept. Prog. Phys.* **57**, 325 (1994).
- [14] V. B. Semikoz and D. D. Sokoloff, *Int. J. Mod. Phys. D* **14**, 1839 (2005).
- [15] L. M. Widrow, *Rev. Mod. Phys.* **74**, 775 (2003) [arXiv:astro-ph/0207240].
- [16] T. Kobayashi, R. Maartens, T. Shiromizu and K. Takahashi, *Phys. Rev. D* **75**, 103501 (2007) [arXiv:astro-ph/0701596].
- [17] A. Brandenburg, K. Enqvist and P. Olesen, *Phys. Rev. D* **54**, 1291 (1996) [arXiv:astro-ph/9602031].
- [18] C. Caprini and R. Durrer, *Phys. Rev. D* **65**, 023517 (2002) [arXiv:astro-ph/0106244].
- [19] A. Kosowsky, T. Kahniashvili, G. Lavrelashvili and B. Ratra, *Phys. Rev. D* **71**, 043006 (2005) [arXiv:astro-ph/0409767].
- [20] C. Caprini and R. Durrer, *Phys. Rev. D* **72**, 088301 (2005) [arXiv:astro-ph/0504553].
- [21] P. P. Avelino and E. P. S. Shellard, *Phys. Rev. D* **51**, 5946 (1995).
- [22] K. Dimopoulos, *Phys. Rev. D* **57**, 4629 (1998) [arXiv:hep-ph/9706513].
- [23] A. C. Davis and K. Dimopoulos, *Phys. Rev. D* **72**, 043517 (2005) [arXiv:hep-ph/0505242].
- [24] E. R. Harrison, *Mon. Not. astr. Soc* **147**, 279 (1970).
- [25] Martin J. Rees, *Q. Jl R. astr. Soc* **28**, 197 (1987).
- [26] Caldwell, R.R. & Allen, B. 1992, *PhysRevD*, **45**, 3447

- [27] C. J. A. P. Martins and E. P. S. Shellard, Phys. Rev. **D54** 2535 (1996), hep-ph/9602271; Phys. Rev. **D53** R575 (1996), hep-ph/9507335; Phys. Rev. **D65** 043514 (2002), hep-ph/0003298.
- [28] S. H. Tye, I. Wasserman and M. Wyman, Phys. Rev. D **71**, 103508 (2005) [Erratum-ibid. D **71**, 129906 (2005)] [arXiv:astro-ph/0503506].
- [29] M. Wyman, L. Pogosian and I. Wasserman, Phys. Rev. D **72**, 023513 (2005) [Erratum-ibid. D **73**, 089905 (2006)] [arXiv:astro-ph/0503364].
- [30] U. Seljak, A. Slosar and P. McDonald, JCAP **0610**, 014 (2006) [arXiv:astro-ph/0604335].
- [31] N. Bevis, M. Hindmarsh, M. Kunz and J. Urrestilla, arXiv:astro-ph/0702223.
- [32] X. Siemens, V. Mandic and J. Creighton, Phys. Rev. Lett. **98**, 111101 (2007) [arXiv:astro-ph/0610920].
- [33] M. R. DePies and C. J. Hogan, Phys. Rev. D **75**, 125006 (2007) [arXiv:astro-ph/0702335].
- [34] K. J. Mack, D. H. Wesley and L. J. King, arXiv:astro-ph/0702648.
- [35] K. Kuijken, X. Siemens and T. Vachaspati, arXiv:0707.2971 [astro-ph].
- [36] L. Pogosian, S. H. Tye, I. Wasserman and M. Wyman, Phys. Rev. D **68**, 023506 (2003) [Erratum-ibid. D **73**, 089904 (2006)] [arXiv:hep-th/0304188].
- [37] U. Seljak and A. Slosar, Phys. Rev. D **74**, 063523 (2006) [arXiv:astro-ph/0604143].
- [38] L. Pogosian, I. Wasserman and M. Wyman, arXiv:astro-ph/0604141.
- [39] C. J. Hogan, Phys. Rev. D **74**, 043526 (2006) [arXiv:astro-ph/0605567].
- [40] X. Siemens, J. Creighton, I. Maor, S. Ray Majumder, K. Cannon and J. Read, Phys. Rev. D **73**, 105001 (2006) [arXiv:gr-qc/0603115].
- [41] T. Vachaspati and A. Vilenkin, Phys. Rev. Lett. **67**, 1057 (1991).
- [42] T. Vachaspati, Phys. Rev. D **45**, 3487 (1992).
- [43] M. B. Hindmarsh and T. W. B. Kibble, Rept. Prog. Phys. **58**, 477 (1995) [arXiv:hep-ph/9411342].
- [44] D. N. Vollick, Phys. Rev. D **45**, 1884 (1992).
- [45] Vilenkin, A. & Shellard, E.P.S. 2000, Cosmic Strings and Other Topological Defects (Cambridge:CUP)
- [46] A. Avgoustidis and E. P. S. Shellard, Phys. Rev. D **73**, 041301 (2006) [arXiv:astro-ph/0512582].
- [47] D. N. Vollick, Phys. Rev. D **48**, 3585 (1993).
- [48] T. Vachaspati, Phys. Rev. Lett. **57**, 1655 - 1657 (1986).
- [49] A. Stebbins, S. Veeraraghavan, R. H. Brandenberger, J. Silk and N. Turok, Astrophys. J. **322**, 1 (1987).
- [50] L. Pogosian and A. Vilenkin, Phys. Rev. D **70**, 063523 (2004) [arXiv:astro-ph/0405606].
- [51] P. P. Avelino and E. P. S. Shellard, Phys. Rev. D **51**, 369 (1995).
- [52] T. Hara, P. Mahonen, and S. Miyoshi, Ap. J. **412**, 22 (1993).

- [53] J. Polchinski, arXiv:hep-th/0412244.
- [54] E. J. Copeland and N. Turok, Phys. Lett. **B173** (1986) 129.
- [55] S. Chandrasekhar, Astrophys. J. **97**, 255 (1943).
- [56] J. Silk and A. Vilenkin, Phys. Rev. Lett. **53**, 1700 (1984).
- [57] H. Lesch and M. Chiba, arXiv:astro-ph/9411072.
- [58] R. M. Kulsrud, R. Cen, J. P. Ostriker and D. Ryu, Astrophys. J. **480**, 481 (1997) [arXiv:astro-ph/9607141].
- [59] M. S. Turner and L. M. Widrow, Phys. Rev. D **37**, 2743 (1988).
- [60] A. C. Davis, M. Lilley and O. Tornkvist, Phys. Rev. D **60**, 021301 (1999) [arXiv:astro-ph/9904022].
- [61] I. McIvor MNRAS **178**, 85 (1977).
- [62] J. C. Higdon Ap. J. **285**, 109 (1984).
- [63] E. Parker Ap. J. **121**, 491 (1955).
- [64] Ya.B. Zeldovich, A.A. Ruzmaikin and D.D. Sokolov, *Magnetic Fields in Astrophysics* (Gordon and Breach, New York, 1983).
- [65] H. K. Moffatt, “Magnetic Field Generation in Electrically Conducting fluids,” Cambridge University Press, Cambridge, England (1978).
- [66] E. N. Parker, “Cosmological Magnetic fields,” Clarendon, Oxford (1979).
- [67] K. Ferriere and D. Schmitt, Astronomy and Astrophysics, **358**, p.125-143 (2000).
- [68] A.A. Ruzmaikin, D.D. Sokolov and V.I. Turchaninov, Astron. Zh. **57**, 311 (1980) [Sov. Astron. **24**, 182 (1980)].
- [69] K. Dimopoulos and A. C. Davis, Phys. Lett. B **390**, 87 (1997) [arXiv:astro-ph/9610013].
- [70] E. Battaner and H. Lesch, arXiv:astro-ph/0003370.
- [71] J. Polchinski and J. V. Rocha, Phys. Rev. D **74**, 083504 (2006) [arXiv:hep-ph/0606205].
- [72] J. Polchinski and J. V. Rocha, arXiv:gr-qc/0702055.
- [73] F. Dubath and J. V. Rocha, Phys. Rev. D **76**, 024001 (2007) [arXiv:gr-qc/0703109].
- [74] K. D. Olum and V. Vanchurin, Phys. Rev. D **75**, 063521 (2007) [arXiv:astro-ph/0610419].
- [75] V. Vanchurin, K. D. Olum and A. Vilenkin, Phys. Rev. D **74**, 063527 (2006) [arXiv:gr-qc/0511159].
- [76] C. J. A. Martins and E. P. S. Shellard, Phys. Rev. D **73**, 043515 (2006) [arXiv:astro-ph/0511792].
- [77] C. Ringeval, M. Sakellariadou, and F. Bouchet, JCAP **0702**, 023 (2007), astro-ph/0511646.
- [78] J. Polchinski, arXiv:0707.0888 [astro-ph].
- [79] B. Allen and P. Casper, Phys. Rev. D **50**, 2496 (1994) [arXiv:gr-qc/9405005].

- [80] P. Casper and B. Allen, Phys. Rev. D **52**, 4337 (1995) [arXiv:gr-qc/9505018].
- [81] T. Vachaspati and A. Vilenkin, Phys. Rev. D **31**, 3052 (1985).
- [82] R. Durrer, Nucl. Phys. B **328**, 238 (1989).
- [83] B. Allen, P. Casper and A. Ottewill, Phys. Rev. D **51**, 1546 (1995) [arXiv:gr-qc/9407023].
- [84] C. J. Hogan and M. J. Rees, Nature **311** (1984) 109.
- [85] D. N. Spergel *et al.* [WMAP Collaboration], arXiv:astro-ph/0603449.
- [86] A. A. Ruzmaikin, D. D. Sokolov, and V. I. Turchaninov, Astron. Zh. **57**, 311 (1980).
- [87] D. Bennett and F. Bouchet, Phys. Rev. Lett. **60** 257 (1988); Astrophys. J. **354** L41 (1990); in *The Formation and Evolution of Cosmic Strings*, proceedings of the Symposium, Cambridge, England 1989, edited by G. W. Gibbons, S. W. Hawking, and T. Vachaspati (Cambridge University Press, Cambridge England 1989); Phys. Rev. D **41** 2408 (1990)

Parameter	Value	Source	description, first used in (equation)
$G\mu_0$	$2 \times 10^{-7}$	[29, 30]	string mass/length
$\mu$	$1.9\mu_0$	[45], radiation era	effective mass/length (2.3)
	$1.5\mu_0$	[45], matter era	
$\alpha$	0.01	[26, 45]	size of large loop/horizon (3.4)
$f_r$	0.7	[87, 26]	loop redshifting energy loss (3.4)
$\tilde{\alpha}$	$f_r\alpha H^{-1}(t_F)/t_F$	Defined in (4.13)	new loop length over formation time
$\Gamma_\ell$	50 (★)		efficiency of grav. wave emission [43] (3.4)
	$50 \lesssim \Gamma_\ell \lesssim 100$	[79]	
	$45 \lesssim \Gamma_\ell \lesssim 55$	[80]	
	50, 80	[26, 82, 84]	
$\Gamma_{gr}$	5	[82]	grav. wave emission yielding torque (A.16)
$\Gamma_p$	10	[83, 81, 82]	rocket effect (A.4)
$\Gamma_{dy}$	0.2 Gyr (★)		dynamo efficiency (4.5)
	$0.2 < \Gamma_{dy}^{-1}/\text{Gyr} < 0.8$	[86, 60]	
	$\Gamma_{dy}^{-1} \gtrsim (1.1 - 1.4) \text{ Gyr}$	[15]	
	$\Gamma_{dy}^{-1} = 0.3 \text{ Gyr}$	[68]	
	$\Gamma_{dy}^{-1} = 0.5 \text{ Gyr}$	[64]	
	$\Gamma_{dy}^{-1} = 2.2 \text{ Gyr}$	[67]	
$z_{dec}$	1089	[85]	redshift at decoupling
$z_{gf}$	6	[22]	redshift of galaxy formation
	10 (★)		
$t_{eq}$	$1.6 \times 10^{12} \text{ s} = 51 \text{ kyr}$		time of matter-radiation equality
$t_{dec}$	$1.2 \times 10^{13} \text{ s} = 380 \text{ kyr}$		time of decoupling (4.10)
$t_0$	13.7 Gyr	[85]	age of the universe
$v_{RMS}$	0.60	[41], matter era	RMS velocity in network
$\bar{v}_{RMS}$	0.15	[41], matter era	RMS velocity avg. over corr. length
$\Omega_m h^2$	0.1277	[85]	matter fraction (4.7)
$h$	0.732	[85]	Hubble parameter (4.7)
$\beta$	$1/2 \leq \beta \leq 1$	[23]	(2.7)
$P$	1 (★)	cosmic strings	intercommutation probability
	$10^{-1} \leq P \leq 1$	D-Strings [53]	
	$10^{-3} \leq P \leq 1$	F-Strings [53]	
$c_1$	0.21 (0.2475)	[27, 28]	VOS parameters in radiation (matter) era
$c_2$	0.18 (0.3675)		
$c_3$	0.28		

**Table 2:** Our parameters. When several values are given, we select the one marked by a (★).